

Internally ratiometric fluorescent sensors for evaluation of intracellular GTP levels and distribution

Anna Bianchi-Smiraglia^{1,6}, Mitra S Rana^{2,5,6}, Colleen E Foley¹, Leslie M Paul¹, Brittany C Lipchick¹, Sudha Moparthy¹, Kalyana Moparthy¹, Emily E Fink¹, Archis Bagati^{1,5}, Edward Hurley³, Hayley C Affronti⁴, Andrei V Bakin⁴, Eugene S Kandel¹, Dominic J Smiraglia⁴ , Maria Laura Feltri³, Rui Sousa²  & Mikhail A Nikiforov¹ 

GTP is a major regulator of multiple cellular processes, but tools for quantitative evaluation of GTP levels in live cells have not been available. We report the development and characterization of genetically encoded GTP sensors, which we constructed by inserting a circularly permuted yellow fluorescent protein (cpYFP) into a region of the bacterial G protein FeoB that undergoes a GTP-driven conformational change. GTP binding to these sensors results in a ratiometric change in their fluorescence, thereby providing an internally normalized response to changes in GTP levels while minimally perturbing those levels. Mutations introduced into FeoB to alter its affinity for GTP created a series of sensors with a wide dynamic range. Critically, in mammalian cells the sensors showed consistent changes in ratiometric signal upon depletion or restoration of GTP pools. We show that these GTP evaluators (GEVALs) are suitable for detection of spatiotemporal changes in GTP levels in living cells and for high-throughput screening of molecules that modulate GTP levels.

GTP regulates a large array of cellular processes ranging from protein synthesis¹ to cell signaling^{2,3}, including activation of G proteins, dysfunction of which underlies a variety of human diseases^{4–6}, most notably cancer⁷. While the need for a method of measuring GTP levels in live cells is clear, no such method currently exists.

We report here the construction of genetically encoded GTP sensors based on fluorescent protein (FP) technology. These sensors exhibit a rapid, internally normalized ratiometric change in fluorescence upon changes in GTP concentration *in vitro* and *in vivo*. They also reveal heterogeneity in the intracellular distribution of GTP, raising the possibility that such variation could regulate the activity of G proteins in different cellular compartments.

RESULTS

Construction of the GTP sensor

The G-protein domain of the *Escherichia coli* iron-transport protein FeoB contains a loop (amino acid residues 35–40) that undergoes a conformational change upon GTP binding⁸ (Fig. 1a,b). As a bacterial protein, FeoB is unlikely to interact specifically with eukaryotic proteins that could confound its function as a GTP sensor. The GTP on and off rates of FeoB are $\sim 10^6 \text{ M}^{-1} \text{ s}^{-1}$ and 12 s^{-1} , respectively⁹, so it can respond quickly to changes in GTP concentration, and its GTP hydrolysis rate is only 0.0015 s^{-1} , so its hydrolysis activity should not reduce local GTP pools.

DNA encoding cpYFP (ref. 10) was inserted into DNA encoding residues 35–40 of the FeoB G-protein domain (Fig. 1c). Fusion nomenclature followed the form “FY1a+1a”: the number designates the insertion site, with “1” corresponding to insertion after residue 35 and “6” to insertion after residue 40; the first “a” indicates the presence of a Ser-Ala-Gly linker at the cpYFP N terminus; the second “a” indicates a Gly-Thr linker at the cpYFP C terminus. Most of the 24 fusions we generated changed fluorescence upon binding GTP, with three (FY1+1a, FY5a+5a and FY6+6a) showing a more than twofold decrease in emission when excited at 485 nm (Supplementary Fig. 1). However, only FY5a+5a showed a ratiometric change, with GTP causing a decrease in fluorescence when the fusion protein was excited at <450 nm and an increase at >450-nm excitation (Supplementary Fig. 2a), resulting in a large change in the ratio of emission intensities at 405-nm and 485-nm excitation (Ex405/Ex485; Fig. 1d). Such ratiometric changes enable researchers to normalize the signal and correct for variations in sensor levels by measuring the ratio of fluorescence at two wavelengths. The ratiometric signal of FY5a+5a is large, ranging from 1.7 to 5.3 across the relevant pH range (Supplementary Fig. 3). For comparison, this signal is over twofold greater than signals achieved by the Perceval¹¹ and

¹Department of Cell Stress Biology, Roswell Park Cancer Institute, Buffalo, New York, USA. ²Department of Biochemistry and Center for Biomedical Neuroscience, University of Texas Health Science Center at San Antonio, San Antonio, Texas, USA. ³Department of Biochemistry and Neurology, Hunter James Kelly Research Institute, Jacobs School of Medicine and Biomedical Sciences, State University of New York at Buffalo, Buffalo, New York, USA. ⁴Department of Cancer Genetics, Roswell Park Cancer Institute, Buffalo, New York, USA. ⁵Present addresses: NICHD, NIH, Bethesda, Maryland, USA (M.S.R.); Department of Cancer Immunology and Virology, Dana-Farber Cancer Institute, Harvard Medical School, Boston, Massachusetts, USA (A.B.). ⁶These authors contributed equally to this work. Correspondence should be addressed to M.A.N. (mikhail.nikiforov@roswellpark.org) or R.S. (sousa@uthscsa.edu).

ATeam¹² sensors, which report on cellular ATP/ADP ratio and ATP levels, respectively.

The sensor is selective for GTP and dGTP

Although 4 μM GTP was sufficient to induce a large change in FY5a+5a fluorescence (Fig. 1d and Supplementary Fig. 2a), even 500 μM UTP, CTP, or GMP had little effect, and these nucleotides did not significantly interfere with the GTP-induced change when they were present in fivefold excess of GTP (Fig. 1d and Supplementary Fig. 2b–g). High concentrations of ATP and inosine triphosphate (ITP) had small effects on fluorescence but, even at 500 μM , induced less than 10% of the change in the Ex400/Ex485 ratio induced by 100 μM GTP and did not markedly affect the changes induced by GTP even when present in fivefold excess of GTP (Fig. 1d and Supplementary Fig. 2h–k).

In contrast, dGTP had effects indistinguishable from GTP (Fig. 1d and Supplementary Fig. 2l). However, even in proliferating cells, dGTP levels are 100-fold lower than GTP levels¹³, so the potential for dGTP to interfere with GTP sensing in cells is negligible.

Fluorescence was also affected by GDP, though the change in Ex400/Ex485 ratio induced by GDP was about fivefold smaller, and required about fivefold higher concentrations, than that induced by GTP (Fig. 1d and Supplementary Fig. 2m). Because GDP has the greatest potential to interfere with GTP sensing, we carried out more extensive interference experiments with GDP/GTP ratios varying from 1:10 to 10:1. Under conditions where GTP addition induced a threefold change in Ex400/Ex485, addition of fourfold excess GDP reduced this change by less than 10%, and addition of greater amounts of GDP reduced this change by a maximum of 25% (Supplementary Fig. 4). Given that, even under extreme starvation conditions, cellular GTP levels exceed GDP levels by severalfold^{13,14}, these data indicate that GDP will not interfere with intracellular sensing of GTP.

The sensor responds rapidly to changes in GTP levels

We measured the kinetics of the response to GTP binding by reacting GTP-free FY5a+5a with GTP in a stop-flow fluorometer. Both the GTP-induced decrease in fluorescence at 485-nm excitation and the increase at 400-nm excitation were fast, with half-lives of 6 ms at 500 μM GTP and 10 ms at 100 μM GTP (Fig. 2a). To measure the rate of the GTP-dissociation-dependent response, FY5a+5a premixed with 100 μM GTP was reacted with 2.5 mM GDP. The presence of GDP in 25-fold excess causes most sensors that release GTP to rebind GDP, so we were able to monitor GTP release by following the reversal of the fluorescence changes induced by the triphosphate. The GTP-dissociation-dependent changes were also fast, with half-lives of ~120 ms (Fig. 2b). While it is unclear why the data do not always obey single-phase exponential functions, they do show that the fluorescence responses are fast, occurring with half-lives of ~10 and ~100 ms in response to, respectively, increases or decreases in GTP concentrations. To determine bleaching kinetics, FY5a+5a, with or without GTP, was continuously exposed to either 400-nm or 485-nm light. After more than 10 min, emission had decreased by less than 0.5% (Ex485) or less than 0.2% (Ex400) in the absence of GTP and by even less in the presence of GTP (Fig. 2c).

Cellular magnesium levels do not affect sensor function

Since GTP binds FeoB in complex with Mg^{2+} , variations in Mg^{2+} concentration could affect sensor fluorescence. We measured the

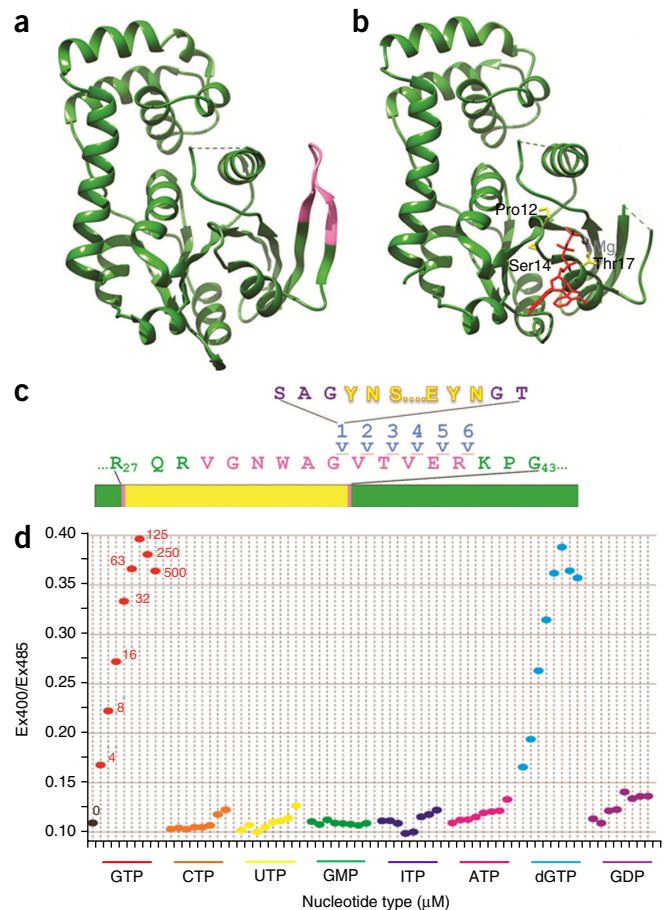


Figure 1 | Construction and nucleotide selectivity of a GTP sensor.

(a) The G protein domain of *E. coli* FeoB without ligand (PDB 3HYR)⁸. The V30-R40 switch I region that undergoes a conformational change upon ligand binding is highlighted in pink. (b) The G protein domain of *E. coli* FeoB protein with a bound GTP analog (shown in red with the Mg^{2+} ion in gray; PDB 3HYT). Amino acid side chains mutated to alter GTP affinity (Pro12, Ser14, and Thr17) are shown in stick representation and colored yellow. The switch I region is not visible in the crystal structure because it becomes disordered upon binding GTP. (c) Sensor construction. We created 24 distinct fusions by inserting cpYFP (yellow) at six different positions (after residues 35–40) within the switch I region (pink) of the FeoB G-protein domain (green), either with or without a Ser-Ala-Gly linker (purple) at the N-terminal fusion point and either with or without a Gly-Thr linker (purple) at the C-terminal fusion point. The lines indicate insertion of cpYFP after residue 35. (d) Ex405/Ex485 ratio for FY5a+5a in the presence of no nucleotide (“0”; black) or the indicated nucleotides (4, 8, 16, 32, 65, 125, 250, and 500 μM of each nucleotide).

effect of varying Mg^{2+} concentration with and without GTP. With 0.1 mM EDTA and no Mg^{2+} , GTP failed to induce a change in sensor fluorescence (Fig. 2d,e, red traces). Addition of 0.25 mM Mg^{2+} (yielding 0.15 mM free Mg^{2+} after chelation by EDTA) partially restored the GTP-induced change in the 400/485 ratio, and addition of 0.5 mM Mg^{2+} (yielding 0.4 mM free Mg^{2+} after chelation) restored 85% of the change. The Ex400/Ex485 ratios varied less than 5% when free Mg^{2+} ranged from 0.9 mM to 3.9 mM, but higher Mg^{2+} (>7.9 mM) reduced this ratio owing to increases in fluorescence at longer excitation wavelengths (Fig. 2d). Without GTP, excitation spectra did not vary with Mg^{2+} concentrations in the 0- to 3.9-mM range, but they showed emission increases at longer excitation wavelengths when the Mg^{2+} concentration

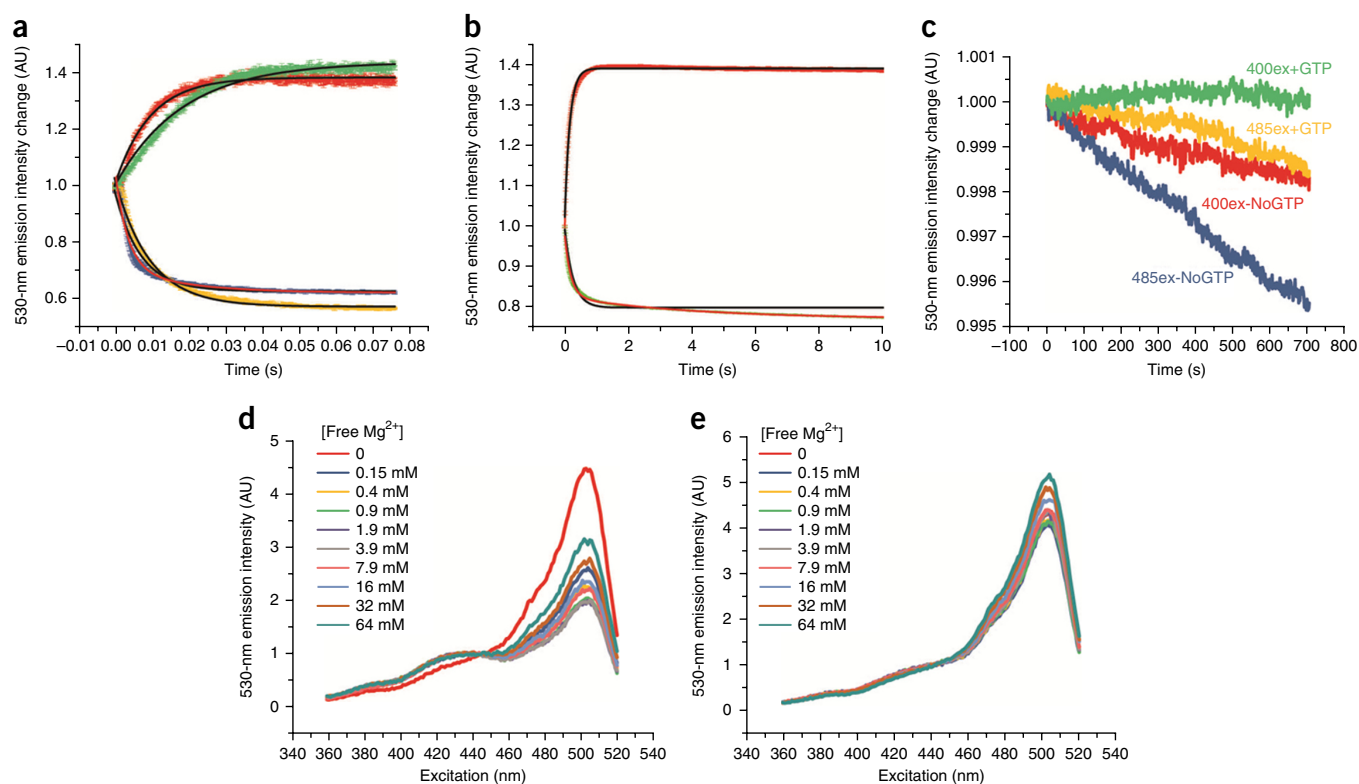


Figure 2 | Kinetics and magnesium dependence of GTP-induced fluorescence changes. (a) Fluorescence emission intensity (530 nm) upon excitation at 400 nm (red and green traces) or 485 nm (blue and yellow traces) over time, for reactions in which the GTP-free FY5a+5a fusion was reacted with 100 μM GTP (green and yellow) or 500 μM GTP (red and blue). Black lines show fits to single-phase exponential association functions (red and green traces) or exponential decay functions (blue and yellow traces). The data for high GTP concentrations at 485-nm excitation (blue trace) was not well fit by a single-phase exponential, so a fit with a double-phase exponential decay function (red line) is also shown. (b) Emission intensity upon excitation at 400 nm (green trace) or 485 nm (red trace) for reactions in which FY5a+5a with 100 μM GTP was reacted with 2.5 mM GDP. As in a, the black and red lines show single-phase and double-phase exponential fits, respectively. (c) Emission intensity for FY5a+5a continuously illuminated at either 400 nm (green and red traces) or 485 nm (yellow and blue traces), either with (green and yellow traces) or without (red and blue traces) GTP. Emission intensity decreases (bleaching) were all $<0.5\%$ over more than 10 min of constant excitation. In a–c, initial fluorescence intensities were normalized to a value of 1.0, and trace thickness shows \pm s.e.m. for $n = 4$ independent replicates. (d,e) Emission intensity plotted against excitation wavelength for FY5A+5A with 100 μM GTP (d) or for GTP-free FY5A+5A (e). Reactions contained 0.1 mM EDTA and the indicated concentrations of Mg^{2+} . Mg^{2+} concentrations are expressed to two significant figures and correspond to free Mg^{2+} concentrations upon chelation by EDTA.

is >7.9 mM (Fig. 2e). These data indicate that Mg^{2+} is required for the GTP-induced change in fluorescence and that very high Mg^{2+} concentrations affect fluorescence independently of GTP. However, both with and without GTP, fluorescence is effectively constant over the Mg^{2+} concentration ranges of 0.5–5 mM that prevail *in vivo*¹⁵.

A set of GTP sensors with a wide dynamic range

The K_d for FeoB binding to GTP is ~ 4 – 15 μM (refs. 9,13), but total cellular GTP is typically 300–800 μM (ref. 13). The tight GTP binding of FeoB could render the sensor insensitive to changes in GTP concentration across physiologically relevant ranges. We therefore created five FY5a+5a variants by introducing mutations to weaken or eliminate GTP binding. We characterized the effective affinities of these fusions for GTP and the most structurally similar cellular ligands (ATP and GDP; Supplementary Fig. 5 and Table 1). The K_{eff} values (GTP concentrations required to obtain 50% of the maximal ratiometric signal) for the five GTP-binding variants ranged from 30 to 2,000 μM . The variant mutated to abolish GTP binding showed no response to GTP. We named these fusions GTP evaluators, or GEVALs, with a numbered suffix

indicating their GTP K_{eff} value (Table 1). The nonbinding variant is named GEVALNull.

GEVAL fluorescence is affected by pH (Supplementary Figs. 3 and 6–8), a feature common to FP-based ligand sensors¹⁶. Fluorescent pH sensors or pH-sensitive dyes are often deployed in parallel with ligand sensors to determine whether a change in sensor fluorescence is due to a change in pH or a change in ligand concentration¹¹. For GEVALs, the most effective control for pH effects is GEVALNull, since it does not respond to GTP but should respond exactly like the other GEVALs to pH or any other change in the cell environment. If GEVAL fluorescence changes are observed under conditions where GEVALNull fluorescence is constant, then they can be attributed to changes in GTP levels rather than to other effects. To confirm that GEVALNull responds to pH identically to the GTP-sensing fusions, we measured their Ex400/Ex485 ratios as a function of pH and GTP concentration (Supplementary Fig. 7). Without GTP, all the GEVALs exhibited equal Ex400/Ex485 ratios that varied identically as pH varied from 5.5 to 8.5. Upon GTP addition, the ratios increased for all the GEVALs except GEVALNull, with the largest increases seen for the sensors with the highest GTP affinity (Supplementary Fig. 7a–e).

Table 1 | GTP and GDP K_{eff} values for the ligand-dependent ratiometric fluorescence changes of mutated sensors

Foeb mutation	GTP K_{eff} (μM)	GDP K_{eff} (μM)
Wild type (GEVAL30)	33.2 \pm 0.3	100 \pm 6
P12G (GEVAL260)	260 \pm 20	1,000 \pm 200
P12G S14A (GEVAL530)	528 \pm 20	1,280 \pm 200
P12G T17S (GEVAL1150)	1,150 \pm 100	2,770 \pm 300
P12G S14A T17S (GEVAL2300)	2,300 \pm 100	3,700 \pm 300
P12A S14A T17A (GEVALNull)	NA	NA

NA, not applicable.

However, the Ex400/Ex485 ratio for GEVALNull remained invariant upon GTP addition (**Supplementary Fig. 7**). The GEVAL sensors were expressed well in *E. coli*, with no indication of aggregation, but to evaluate this further we measured their apparent molecular weight and polydispersity by dynamic light scattering and found them to be monomeric and monodisperse in solution (**Supplementary Fig. 8b**).

GEVAL sensor response to GTP depletion

We used lentiviral transduction to express GEVAL30, GEVAL530 and GEVALNull (the high- and medium-affinity GTP sensors and the unresponsive negative control, respectively) in SK-Mel-103 human melanoma cells. We verified equivalent expression of all sensors

by immunofluorescence and immunoblotting (**Fig. 3a**). Cells were then transiently transfected with the pHRed¹⁷ vector (with over 90% efficiency) to control for pH variations (**Supplementary Fig. 9a**). Experiments showing that the sensors do not affect cellular GTP levels and are not affected by autofluorescence and bleed-through are described in **Supplementary Note 1**.

To assess the sensors' sensitivity, we treated cells expressing GEVAL and pHRed sensors with various concentrations of mycophenolic acid (MPA, an inhibitor of the IMPDH1 and IMPDH2 enzymes involved in synthesis of the GMP precursor XMP) for 48 h to deplete GTP and calculated the Ex405/Ex488 ratio for the GTP sensors and the Ex594/Ex458 ratio for pHRed. To transform the Ex594/Ex458 ratios into pH values, we interpolated underlying data from ref. 17 (Online Methods). The analysis showed no difference in overall cell pH among all populations (**Supplementary Fig. 10a,b**). We verified the functionality of the pHRed sensor by monitoring its response to changes in the pH of the cell medium via addition of NH_4Cl (20 mM final) followed by acetic acid (10 mM final) as previously described¹⁷ (**Supplementary Fig. 10c,d**).

Importantly, fluorometric ratios of GEVAL30 and GEVAL530 decreased in response to MPA, while GEVALNull did not show any significant difference (**Figs. 3b,c**). Similar results were obtained in 1 \times and 5 \times cells (**Supplementary Fig. 9c,g**). Depletion of GTP pools by MPA was verified in parallel by HPLC (**Fig. 3d**).

The Ex405/Ex488 ratio of GEVAL30 was highest in the absence of MPA (1.24), which suggests that this sensor is effectively GTP saturated *in vivo*. This ratio decreased in parallel with GTP depletion by MPA to 1.0 (77% of the original value). GEVAL530's Ex405/Ex488

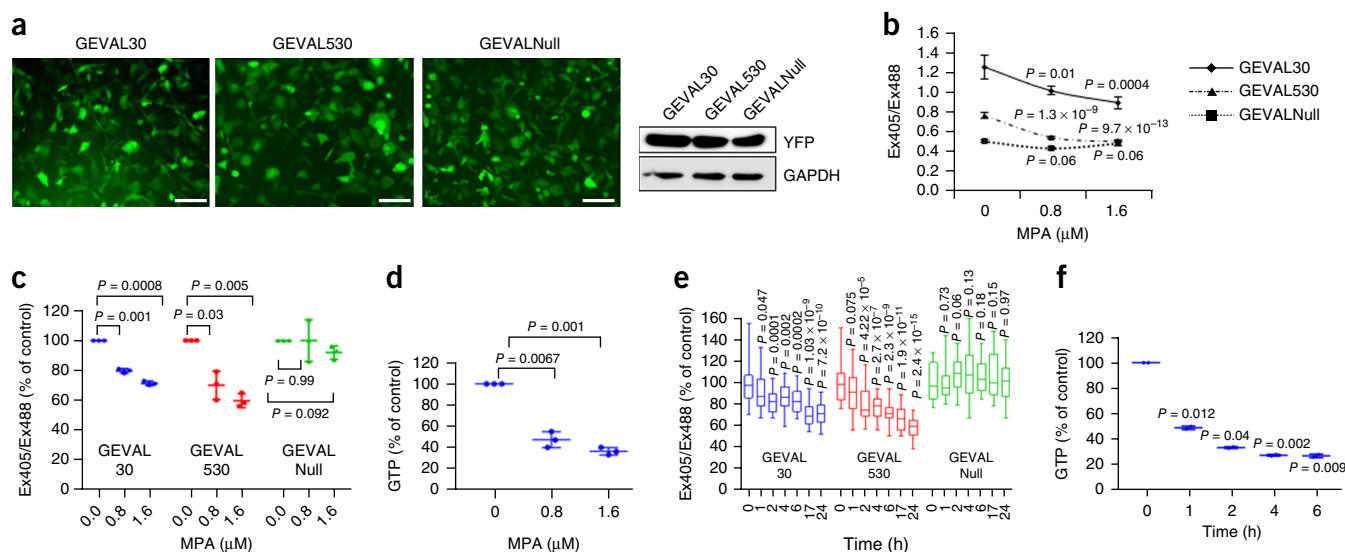


Figure 3 | Validation of the GEVAL sensors' GTP-sensing activity in mammalian cells. **(a)** Expression of sensors in SK-Mel-103 cells was evaluated by immunofluorescence (left; scale bar, 100 μm) and immunoblotting with anti-YFP (right; GAPDH was used to verify equal loading). **(b)** SK-Mel-103 cells expressing GEVAL sensors were plated on coverslip chambers, treated for 48 h with the indicated concentrations of MPA and imaged as described in the Online Methods. We analyzed 30 cells in each population with ImageJ to calculate the Ex405/Ex488 ratio. Means \pm s.e.m. are plotted. **(c)** Dot plot of three independent experiments as in **b** normalized to the untreated control in each group; dots represent single experiments, horizontal bars represent the mean, and vertical lines show s.d. **(d)** Dot plot as in **c** (three independent experiments) showing GTP levels measured by HPLC in GEVAL-expressing SK-Mel-103 cells treated with MPA. **(e)** Cells as in **b,c** were imaged at 0 h, then treated with 1.6 μM MPA and imaged again at the indicated time points. Bar-and-whisker plots show results from 30 cells in two independent experiments, normalized to the untreated control (0 h); horizontal bars represent the mean, whiskers represent minimum and maximum values, and boxes represent the first and third quartiles. **(f)** Dot plot as in **c,d** (two independent experiments) showing GTP levels measured by HPLC in SK-Mel-103 cells treated with 1.6 μM MPA for the indicated times. *P* values were calculated with the two-tailed Student's *t*-test.

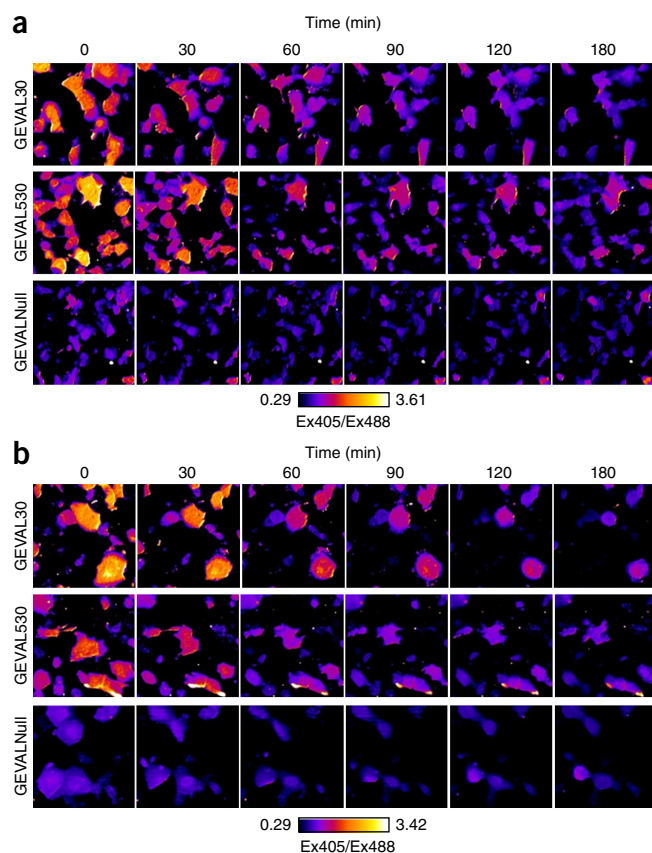


Figure 4 | Detection of spatiotemporal variation of GTP levels in cells. (a,b) SK-Mel-103 cells expressing GEVAL30, GEVAL530 or GEVALNull were plated on coverslip chambers and imaged as described in the Online Methods (0 h). Cells were then treated with 1.6 μM MPA (a) or 25 μM mizoribine (b) and imaged again at the indicated time points. Pixel-by-pixel ratiometric images were generated within ImageJ with the RatioPlus Plugin for each time point. All the ratios were then combined in a stack to ensure a uniform application of contrast enhancement and false coloring (with the FIRE_LUT tool). Representative false-colored ratiometric images are shown. The Ex405/Ex488 ratio over time in ten cells per population is presented in **Supplementary Figure 11d,e**.

ratio in untreated cells was lower than that of GEVAL30 (0.75 versus 1.24), suggesting that this weaker sensor is only partially saturated with GTP. The GEVAL530 sensor became apparently void of GTP as the concentration of MPA increased, reaching the same Ex405/Ex488 ratio as the GEVALNull sensor (0.5), which exhibited the lowest ratio irrespective of MPA treatment (**Fig. 3b**). Similar results were obtained with another inhibitor of IMPDH1 and IMPDH2, mizoribine¹⁸ (**Supplementary Fig. 11a,b**).

Spatio-temporal changes in response to GTP depletion

GEVAL-expressing cell populations were imaged at different times after treatment with 1.6 μM MPA (**Fig. 3e**). GEVAL30 and GEVAL530 quickly responded to MPA, reaching Ex405/Ex488 values within 4–6 h that were similar to the ratio after long-term treatment (48 h; compare **Fig. 3c,e**). GEVALNull activity was unaffected (**Fig. 3e**). HPLC was measured in parallel up to 6 h (**Fig. 3f**), at which point GTP depletion was comparable to that achieved after longer MPA treatments (**Fig. 3d**).

Next, we imaged individual GEVAL-expressing cells at 30-min intervals after MPA treatment. Cell imaging was followed by pixel-by-pixel calculation of the Ex405/Ex488 ratio and false coloring. The Ex405/Ex488 ratios for GEVAL30 and GEVAL530 decreased rapidly over time (**Fig. 4a** and **Supplementary Fig. 11d**). We obtained similar results with mizoribine (**Fig. 4b** and **Supplementary Fig. 11c,e**).

We also used ratiometric imaging to assess intracellular variations in GEVAL sensor activity. Cells expressing GEVALNull showed a uniformly low ratio throughout each cell, whereas both GEVAL530 and GEVAL30 cells had pockets with higher and lower Ex405/Ex488 ratios (**Fig. 5a**). We also analyzed individual sensors to reveal the dynamic range of each sensor, which allowed us to calculate the exact ratios for different subcellular regions displaying a high or low ratio (**Fig. 5b**).

The distributions of per-pixel signal ratios within individual cells harboring GEVAL30 and GEVAL530 had significantly higher skewness values ($P < 10^{-5}$ for GEVAL30; $P < 0.05$ for GEVAL530) and excess kurtosis ($P < 10^{-5}$ for both sensors) compared with the cells expressing GEVALNull (**Supplementary Fig. 12a,b**), further suggesting that the distribution of GTP in the cell is heterogeneous. This heterogeneity was not due to pH variations, since similar pH values were observed between areas of high and low GEVAL activity (**Supplementary Fig. 13**).

GEVAL sensors' response to increased GTP levels

Cells were imaged after MPA treatment with or without the addition of 100 μM guanosine (to replenish intracellular GTP levels^{19–21}). MPA treatment decreased the Ex405/Ex488 ratio by up to 34% for GEVAL30 and up to 42% for GEVAL530, and guanosine supplementation fully reversed this effect (**Fig. 5c**). Thus, the GEVAL sensors detected both depletion and replenishment of GTP.

In parallel, we predepleted intracellular GTP pools overnight with MPA, then imaged them before and after treatment with either vehicle or 100 μM guanosine. Within 1 h, addition of guanosine increased the activity of GEVAL30 and GEVAL530 but not GEVALNull (**Fig. 5d**). Guanosine restored the sensors' activity following GTP depletion (**Fig. 5c,d**) but did not increase the basal activity of GEVAL30 and only modestly increased that of GEVAL530 when GTP pools were at their physiological levels (**Fig. 5c**). These data suggest that GEVAL30 is GTP saturated at the GTP concentrations normally found in these cells and that GEVAL530 is only partially saturated.

GEVAL sensors' response to genetic depletion of GTP

To evaluate GEVALs activity in response to genetic depletion of GTP, we transduced cells with a short hairpin RNA (shRNA) that suppresses IMPDH2 expression²² (**Fig. 5e**). IMPDH2 depletion reduced the Ex405/Ex488 ratios of GEVAL30 and GEVAL530 by 16–18%, while GEVALNull's ratio was unaffected (**Fig. 5f**). The smaller reduction compared to MPA inhibition of the sensors was consistent with HPLC data (compare the 34% decrease upon IMPDH2 suppression in **Fig. 5g** with the 53% decrease at 0.8 μM MPA in **Fig. 3d**) and could be due to incomplete shRNA depletion of IMPDH2. Importantly, activity of GEVAL sensors in cells expressing shRNA-resistant IMPDH2 cDNA was not affected by the above IMPDH2 shRNA (**Supplementary Fig. 14a,b**).

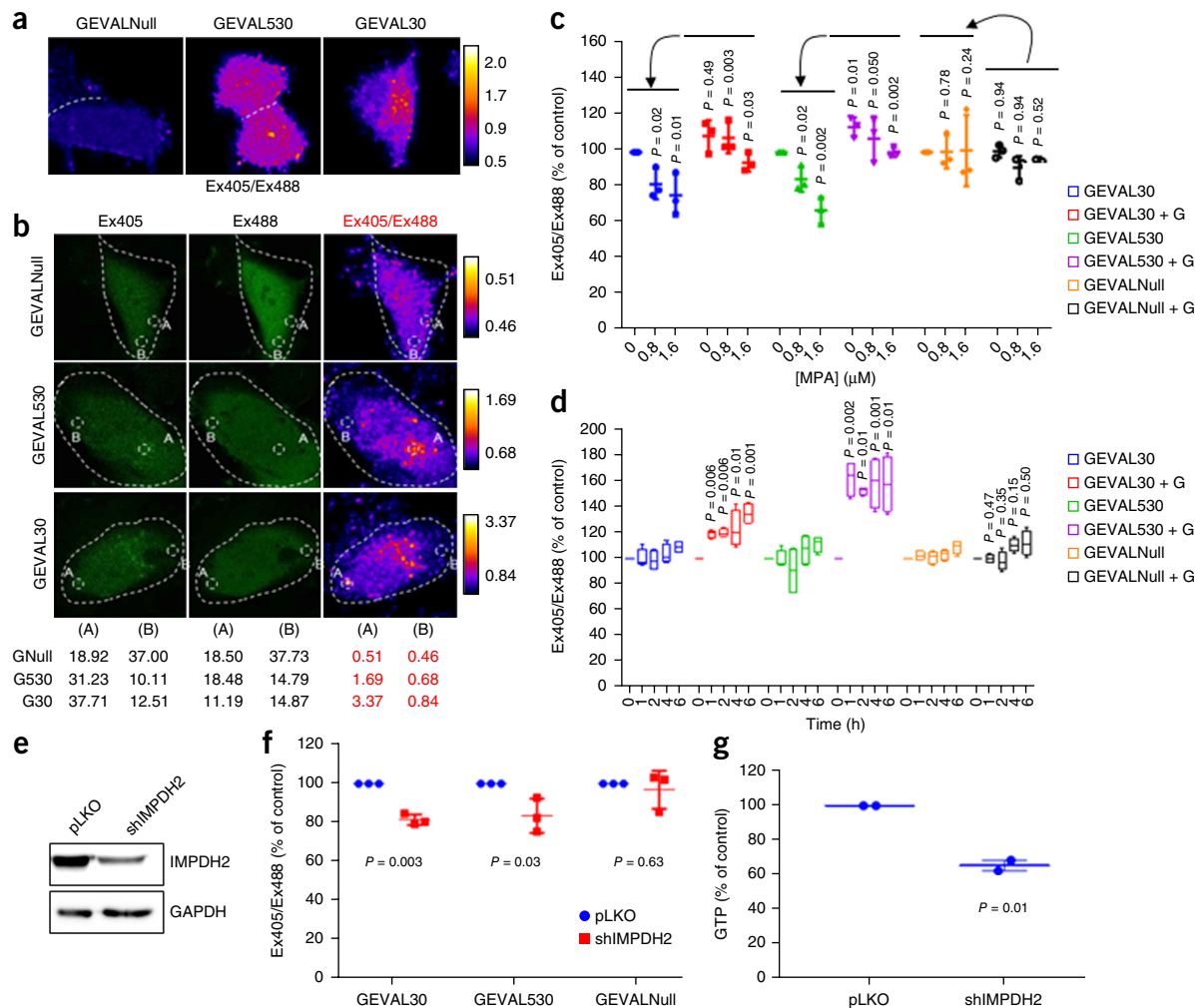


Figure 5 | GEVAL sensors detect GTP gradients in cells and respond to GTP saturation or genetic inhibition. **(a)** False-colored pixel-by-pixel ratiometric images of SK-Mel-103 cells transduced with the three sensors (as in Fig. 4). **(b)** Cell images as in **a**, but with contrast enhancement and false coloring applied independently to each sensor population. Indicated areas of high (A) and low (B) ratios within each image were analyzed with ImageJ to obtain numerical ratio values for the scaling within each image. **(c)** SK-Mel-103 cells transduced with the three sensors were treated for 48 h with MPA in the absence or presence of 100 μM guanosine (+G). Cells were then imaged and the Ex405/Ex488 ratio was calculated for 30 cells per population. Dot plots (as in Fig. 3) show results from three independent experiments normalized to the untreated control in each group. **(d)** Sensor-expressing SK-Mel-103 cells were pretreated overnight with 1.6 μM MPA and imaged (0 h), then treated with 100 μM guanosine or vehicle before further imaging at the indicated times. The Ex405/Ex488 ratio calculated for 30 cells per population is reported as bar-and-whisker plots (as in Fig. 3) from four independent experiments normalized to the untreated control (0 h) in each group. **(e)** SK-Mel-103 cells were transduced with empty vector or with shRNA suppressing IMPDH2. IMPDH2 suppression was verified by immunoblotting, and GAPDH was used to verify equal loading. **(f)** Dot plots of Ex405/Ex488 ratio in IMPDH2-suppressed cells (three independent experiments). **(g)** Dot plots of GTP levels measured by HPLC in IMPDH2-suppressed cells (two independent experiments). All *P* values were calculated with a two-tailed Student's *t*-test.

GEVAL sensors are suitable for high-throughput screening

To assess the sensors' suitability for high-throughput (HTP) screening, we seeded cells expressing GEVAL30 or GEVAL530 in 26 wells of a glass-bottom 96-well plate and treated them with either vehicle or 1.6 μM MPA for 24 h. The center of each well was imaged, ten cells per well were analyzed, and the average of their Ex405/Ex488 ratios was used as the average ratiometric intensity of each well. *Z'* values of 0.51 and 0.15 were calculated for GEVAL30 and GEVAL530, respectively (Supplementary Fig. 14c,d), suggesting that GEVAL sensors can be developed for HTP applications.

DISCUSSION

Monitoring of cellular GTP currently relies on techniques like HPLC²³ or mass spectrometry (MS)²⁴, which cannot be performed in live cells, result in loss of spatial resolution and are prone to artifacts because of the lability of NTPs during extraction^{23,25}. A nanosensor for guanine nucleotides has been constructed via coupling of a dye to an aptamer fused to a graphite sheet²⁶. However, this sensor cannot be used quantitatively, cannot be expressed in cells and does not differentiate between guanine, GMP, GDP and GTP.

The GEVAL sensors deployed in conjunction with pHRES sensors are capable of detecting not only temporal changes in GTP levels in living cells but also changes in subcellular GTP distribution.

In addition, HPLC- or MS-based measurements cannot distinguish between total and free GTP levels. Several recent publications strongly suggest that free GTP levels may be below total levels^{19,27,28}. This is consistent with our observation that GEVAL30 is sensitive to GTP depletion, even though we had expected that this sensor's low K_{eff} for GTP binding might render it insensitive.

Together, our data reveal that the GEVAL sensors represent a novel set of tools that allows semiquantitative assessment of changes in GTP levels within cell populations and in the intracellular distribution of GTP within individual cells.

METHODS

Methods, including statements of data availability and any associated accession codes and references, are available in the [online version of the paper](#).

Note: Any Supplementary Information and Source Data files are available in the online version of the paper.

ACKNOWLEDGMENTS

This work was supported by NIH grants CA151128 and GM118933 (R.S.); CA197996 (D.J.S.); CA120244, CA193981 and CA190533 (M.A.N.); Ruth L. Kirschstein National Research Service Award F32CA189622 (A.B.-S.); NIH grant 1F99CA21245501 (H.C.A.); Empire State Development Corporation Krabbe Disease Research Working Capital X561 and Krabbe Disease Research Capital Equipment U446 (M.L.F.); and the Jennifer Linscott Tietgen Foundation (M.A.N.). The pLV-SV40-puro lentiviral vector was obtained from P. Chumakov (Cleveland Clinic).

AUTHOR CONTRIBUTIONS

A.B.-S., M.S.R., R.S. and M.A.N. designed the experiments and wrote the manuscript; A.B.-S. and M.S.R. performed most of the experiments and analyzed the data; C.E.F., B.C.L., L.M.P., S.M., K.M., E.E.F. and A.B. performed some of the experiments; H.C.A. performed HPLC analysis; E.H. assisted with the microscopy acquisition and analysis; D.J.S., A.V.B., E.S.K. and M.L.F. supervised part of the study; R.S. and M.A.N. conceived the initial hypothesis and supervised the study. A.B.-S. and M.S.R. contributed equally to this study. All authors discussed the results and commented on the manuscript.

COMPETING FINANCIAL INTERESTS

The authors declare no competing financial interests.

Reprints and permissions information is available online at <http://www.nature.com/reprints/index.html>. Publisher's note: Springer Nature remains neutral with regard to jurisdictional claims in published maps and institutional affiliations.

- Shoji, S., Walker, S.E. & Fredrick, K. Ribosomal translocation: one step closer to the molecular mechanism. *ACS Chem. Biol.* **4**, 93–107 (2009).
- Simon, M.I., Strathmann, M.P. & Gautam, N. Diversity of G proteins in signal transduction. *Science* **252**, 802–808 (1991).
- Neves, S.R., Ram, P.T. & Iyengar, R. G protein pathways. *Science* **296**, 1636–1639 (2002).
- MacMicking, J.D. IFN-inducible GTPases and immunity to intracellular pathogens. *Trends Immunol.* **25**, 601–609 (2004).
- Kresse, A. *et al.* Analyses of murine GBP homology clusters based on in silico, in vitro and in vivo studies. *BMC Genomics* **9**, 158 (2008).
- Vestal, D.J. & Jeyaratnam, J.A. The guanylate-binding proteins: emerging insights into the biochemical properties and functions of this family of large interferon-induced guanosine triphosphatase. *J. Interferon Cytokine Res.* **31**, 89–97 (2011).
- Downward, J. Targeting RAS signalling pathways in cancer therapy. *Nat. Rev. Cancer* **3**, 11–22 (2003).
- Guilfoyle, A. *et al.* Structural basis of GDP release and gating in G protein coupled Fe²⁺ transport. *EMBO J.* **28**, 2677–2685 (2009).
- Marlovits, T.C., Haase, W., Herrmann, C., Aller, S.G. & Unger, V.M. The membrane protein FeoB contains an intramolecular G protein essential for Fe(II) uptake in bacteria. *Proc. Natl. Acad. Sci. USA* **99**, 16243–16248 (2002).
- Belousov, V.V. *et al.* Genetically encoded fluorescent indicator for intracellular hydrogen peroxide. *Nat. Methods* **3**, 281–286 (2006).
- Berg, J., Hung, Y.P. & Yellen, G. A genetically encoded fluorescent reporter of ATP:ADP ratio. *Nat. Methods* **6**, 161–166 (2009).
- Imamura, H. *et al.* Visualization of ATP levels inside single living cells with fluorescence resonance energy transfer-based genetically encoded indicators. *Proc. Natl. Acad. Sci. USA* **106**, 15651–15656 (2009).
- Traut, T.W. Physiological concentrations of purines and pyrimidines. *Mol. Cell. Biochem.* **140**, 1–22 (1994).
- Matsushika, A., Nagashima, A., Goshima, T. & Hoshino, T. Fermentation of xylose causes inefficient metabolic state due to carbon/energy starvation and reduced glycolytic flux in recombinant industrial *Saccharomyces cerevisiae*. *PLoS One* **8**, e69005 (2013).
- Romani, A.M. Cellular magnesium homeostasis. *Arch. Biochem. Biophys.* **512**, 1–23 (2011).
- Palmer, A.E., Qin, Y., Park, J.G. & McCombs, J.E. Design and application of genetically encoded biosensors. *Trends Biotechnol.* **29**, 144–152 (2011).
- Tantama, M., Hung, Y.P. & Yellen, G. Imaging intracellular pH in live cells with a genetically encoded red fluorescent protein sensor. *J. Am. Chem. Soc.* **133**, 10034–10037 (2011).
- Turka, L.A., Dayton, J., Sinclair, G., Thompson, C.B. & Mitchell, B.S. Guanine ribonucleotide depletion inhibits T cell activation. Mechanism of action of the immunosuppressive drug mizoribine. *J. Clin. Invest.* **87**, 940–948 (1991).
- Wawrzyniak, J.A. *et al.* A purine nucleotide biosynthesis enzyme guanosine monophosphate reductase is a suppressor of melanoma invasion. *Cell Rep.* **5**, 493–507 (2013).
- Gu, J.J. *et al.* Induction of apoptosis in IL-3-dependent hematopoietic cell lines by guanine nucleotide depletion. *Blood* **101**, 4958–4965 (2003).
- Laliberté, J., Yee, A., Xiong, Y. & Mitchell, B.S. Effects of guanine nucleotide depletion on cell cycle progression in human T lymphocytes. *Blood* **91**, 2896–2904 (1998).
- Mannava, S. *et al.* Direct role of nucleotide metabolism in C-MYC-dependent proliferation of melanoma cells. *Cell Cycle* **7**, 2392–2400 (2008).
- Buckstein, M.H., He, J. & Rubin, H. Characterization of nucleotide pools as a function of physiological state in *Escherichia coli*. *J. Bacteriol.* **190**, 718–726 (2008).
- Chen, P. *et al.* A LC-MS/MS method for the analysis of intracellular nucleoside triphosphate levels. *Pharm. Res.* **26**, 1504–1515 (2009).
- Qiu, Y. *et al.* Mycophenolic acid-induced GTP depletion also affects ATP and pyrimidine synthesis in mitogen-stimulated primary human T-lymphocytes. *Transplantation* **69**, 890–897 (2000).
- Wang, Y., Tang, L., Li, Z., Lin, Y. & Li, J. In situ simultaneous monitoring of ATP and GTP using a graphene oxide nanosheet-based sensing platform in living cells. *Nat. Protoc.* **9**, 1944–1955 (2014).
- Sumita, K. *et al.* The lipid kinase PI5P4K β is an intracellular GTP sensor for metabolism and tumorigenesis. *Mol. Cell* **61**, 187–198 (2016).
- Takeuchi, K. *et al.* Structural reverse genetics study of the PI5P4K β -nucleotide complexes reveals the presence of the GTP bioenergetic system in mammalian cells. *FEBS J.* **283**, 3556–3562 (2016).

ONLINE METHODS

GTP sensor construction. DNA encoding FeoB⁸ was synthesized with codons optimized for mammalian expression and cloned into pET15b (Genscript, NJ). DNA encoding FeoB switch I region was engineered to contain NgoMIV and SmaI sites at codons 34/35 and 41/42. FeoB DNA was PCR amplified with forward and reverse primers containing, respectively, XbaI and HindIII restriction sites, and ligated into XbaI/HindIII digested pRSET A (Invitrogen) from which a single NgoMIV site had been removed by site-directed mutagenesis. DNA coding for cpYFP was PCR amplified from the ATP/ADP ratio sensor Perceval¹¹ (Addgene). For insertion into each position of the FeoB switch I region, we created a total of four PCR products from two forward and two reverse primers that differed in encoding either an additional three (SAG) or two (GT) linker residues at, respectively, the N- or C-terminal points of insertion of the cpYFP. NgoMIV digested PCR products were ligated into NgoMIV/SmaI digested pRSET FeoB plasmid from which the Ngo site had been eliminated. Since the pRSET vectors did not yield strong protein expression, FeoB-cpYFP DNAs were PCR amplified with primers containing NdeI and XhoI restriction sites, digested with NdeI and XhoI and ligated into NdeI/XhoI digested pET32 (EMDMillipore). To generate point mutations in the FeoB component of the sensor to alter its affinity for GTP we performed PCR-mediated mutagenesis using mutagenic primers with the QuikChange Mutagenesis Kit (Stratagene).

Protein expression and purification. pET32 expression vectors were transformed into BL21-DE3 cells and single colonies were grown overnight in Luria Broth with 50 µg/ml ampicillin and used to inoculate larger volumes of 2× YT media at 1:100 dilutions. Cells were grown at 37 °C to an OD₆₀₀ of 0.6–0.8 and induced with 1 mM IPTG, then transferred to 30 °C and grown for 12–18 h. Cells were harvested by centrifugation at 4 °C and the bright yellow-green cell pellets were re-suspended in 50 mM Tris-HCl, pH 8.3, 200 mM NaCl, 0.1% Tween-20, 10 mM imidazole (lysis buffer). Prior to lysis by sonication (Misonix, CT), PMSF was added to 1 mM. Lysates were clarified by 30 min of centrifugation at 15,000g, and the protein was purified from the supernatants on Ni-NTA resin (Qiagen, CA).

Fluorometry. Fluorescence spectra for purified proteins were measured on Horiba JobinYvon Fluoromax-3 or Shimadzu RF-5301PC spectrofluorometers. GEVAL sensors at 1 µM concentration in 100 mM KCl, 50 mM PIPES, pH 7.0, 5 mM MgCl₂, and 10% glycerol (buffer A), and in the presence of varying concentrations of different nucleotides (as specified in individual figure legends; mixed and incubated for 5–10 min at room temperature), were excited at 320 nm to 520 nm at room temperature while emission at 530 nm was measured. For experiments in which the effects of Mg²⁺ concentration were measured, 0.1 mM EDTA was added to buffer A and 1 M MgCl₂ was added to give total Mg²⁺ concentrations of 0, 0.25, 0.5, 1, 2, 4, 18, 16, 32 and 64 mM. The corresponding free Mg²⁺ concentrations after chelation by EDTA are listed in **Figure 2d,e**. Stop-flow fluorometry data were collected at room temperature on an Applied Photosystems stopped-flow fluorometer equipped with an excitation monochromator and a 515-nm log-pass cutoff filter, with excitation at either 400 or 485 nm, and emission measured at 530 nm. Syringes feeding the stop-flow reactant chambers were filled with either 2 µM

GEVAL30 alone or 2 µM GEVAL30 plus 100 µM GTP in buffer A, and then reacted with an equal volume of either 200 µM GTP, 1 mM GTP or 2.5 mM GDP, as indicated in figure legends.

Ligand binding assays. Binding assays were done on a BioTek Synergy 2 plate reader at 28 °C. 10-µl aliquots of ligand (GTP, GDP, ATP) in binding buffer at 10× final concentration were pipetted into a 96-well fluorescence plate, and 90 µl of the GTP sensor protein solution at 1.12 µM was added to give a protein concentration of 1 µM. The plate was read with excitation at 485 or 400 nm and excitation at 528 nm. The ratio of the fluorescence from excitation at the two wavelengths was fit to the following equation:

$$\frac{F_R}{F_0} = F_N = \frac{1 + \frac{[\text{Ligand}]}{K_d}}{1 + \frac{[\text{Ligand}]R}{K_d}}$$

where F_R is the fluorescence ratio (F_{400}/F_{485}) at a given ligand concentration, F_0 is the fluorescence ratio (F_{400}/F_{485}) at zero ligand, F_N is the fluorescence ratio normalized to $F_0 = 1$, K_d is the ligand dissociation constant, $R = (F_0/F_\infty)$, and F_∞ is the fluorescence ratio (F_{400}/F_{485}) at infinite ligand concentration. Kinetic assays were carried out similarly, but with the plate reader set to dispense the sensor and immediately start reading fluorescence at 2-s intervals.

pH dependence of the GTP sensors. The pH dependence of the GTP sensors was measured in 100 mM KCl, 5 mM MgCl₂, 10% glycerol with the following buffering agents in the specified pH ranges: MES (pH 5.5–6.5), PIPES (pH 7), Tris-HCl (pH 7.5–8.5), and glycine-NaOH (pH 9–10); 2 µl of 50 µM protein solutions in water were added to 98 µl of the various pH buffers to give a protein concentration of 1 µM (in the presence or absence of 1 mM GTP), and fluorescence was measured as described for the ligand binding assays.

Dynamic light scattering. We measured dynamic light scattering on a DynaPro Protein Solutions instrument with 50 µl of a 20 µM protein solution and 10⁴ s of acquisition time. Hydrodynamic radii (R_h) and MW were calculated using the DynaPro software assuming an isotropic sphere model and buffer viscosity set to phosphate-buffered saline (PBS) at 25 °C.

Cell lines. SK-Mel-103 human melanoma cell lines were obtained from Sloan Kettering Memorial Cancer Center; HEK293FT were purchased from Clontech (Palo Alto, CA, USA). Cells were cultured in DMEM (Invitrogen, Carlsbad, CA, USA) supplemented with 10% FCS, 2 mM glutamine and penicillin-streptomycin antibiotics. Cells were kept at 37 °C under an atmosphere of 5% carbon dioxide. For cell imaging, 1 h before imaging the cells were rinsed once with PBS and supplemented with an immunofluorescence-compatible media (IFM): FluoroBrite DMEM (Invitrogen) supplemented with 4 mM glutamine, 0.5% FBS, and 20 mM HEPES, pH 7.4. Cell lines were recently authenticated and verified as mycoplasma-free with a MycoAlert mycoplasma detection kit purchased from Lonza (Allendale, NJ, USA; LT07-318).

Antibodies and other reagents. Mycophenolic acid, mizoribine, and guanosine were purchased from Sigma-Aldrich (St. Louis,

MO, USA). The following antibodies were used: mouse monoclonal to GAPDH (Cat. # AM4300, Ambion, Austin, Texas, USA); rabbit polyclonal to IMPDH2 (Cat # HPA001400, Sigma-Aldrich); and mouse monoclonal to GFP/YFP (Cat # sc-9996, Santa Cruz Biotechnology, Santa Cruz, CA, USA). Nunc Lab-Tek chambered coverglass (1.5 mm) were purchased from Thermo Fisher Scientific (Fair Lawn, NJ, USA); 1.5-mm glass bottom 96-well culture plates were purchased from Mattek (Ashland, MA).

Immunoblotting. Whole cell extracts were prepared and analyzed as previously described¹⁹.

Plasmids and infection. The GW1-pHRed, pCMVdeltaR8.2 (DR) and pCMV-VSV-G (VSV-G) vectors were purchased from Addgene (Cambridge, MA, USA). The pLV-SV4-puro lentiviral vector was obtained from Dr. Peter Chumakov, Cleveland Clinic (Cleveland, OH, USA). Lentiviral vectors encoding short-hairpin RNA (shRNA) specific to *IMPDH2* along with a nonsilencing control vector were purchased from Sigma and have been described previously¹⁹. The GEVAL sensors were PCR-amplified from the bacterial expression vectors with the following primers and cloned into the pLVp lentiviral expression system.

GEVAL_FWD (XhoI) CATTGctcgagATGAAAAACTGA CAATCGGACTGA

GEVAL_REV (NheI) CGGTAgctagcTTAGGACACGACA TCGC

The *IMPDH2*-shRNA-resistant vector was created with the Q5 site-directed mutagenesis kit (New England BioLabs, NEB, Ipswich, MA, USA) from our previously generated *IMPDH2* lentiviral expression vector²², using the following primers and following the manufacturer's instructions:

FWD primer gtaccgaggaATGGGTTCTCTCGATGCC

REV primer tttttgagtcgATCCCATCGGAAAAGAAG

The lentiviral infection protocol was described previously²⁹. Briefly, lentiviral supernatants were prepared by transfection of HEK293FT cells with 2.5 μ g of DR, 1 μ g of VSV-G, and 2.5 μ g of target DNA per 60-mm dish, using LipoD293 according to the manufacturer's protocol. Supernatants were collected, filtered through 0.45- μ m filters and used to infect the target cells. All infected cells were briefly selected for resistance to puromycin before use in the described assays.

Nucleotide quantification. Nucleotide quantification was performed as previously described^{19,30}. Briefly, cells were harvested by trypsinization, extracted with 0.4 N perchloric acid and neutralized. NTPs were separated and quantified using a strong anion exchange column (Sigma-Aldrich, St. Louis, MO) assembled on the Waters 2796 Bioseparation module controlled by Empower 3 software at the Bioanalytics, Metabolomics, and Pharmacokinetics Core Facility at Roswell Park Cancer Institute. Nucleotides were eluted with a linear gradient of 80% 0.005 M ammonium phosphate, pH 2.8, and 20% 0.75 M ammonium phosphate, pH 3.7, to 20% 0.005 M ammonium phosphate, pH 2.8 and 80% 0.75 M ammonium phosphate, pH 3.7 over 30 min, which was then maintained for an additional 5 min. The mobile phase was then returned to starting conditions over 10 min, and equilibrated for an additional 30 min before the next injection. Nucleotides were identified based on their UV absorbance spectrum and quantified at either 254 or 281 nm by comparison to the absorbance of a known amount of authentic standard.

Cell imaging acquisition and analysis. Cells were imaged with a Leica AOBSP5 confocal equipped with a multi-line Argon laser, a 405 diode laser, and a 594 helium-neon laser, with a 40 \times immersion lens (except for the HTP screening test, were a 20 \times dry lens was used). The microscope is regularly checked by Leica representatives during visits covered by the service contract. The GTP sensors were excited sequentially with the 405-nm wavelength of the diode laser and the 488-nm line of the argon laser and fluorescence emission was collected from 502 nm to 544 nm. The pHRed sensor was excited sequentially with the 458-nm line of the argon laser and the 594-nm helium-neon laser and fluorescence emission was collected from 598 nm to 647 nm. Thus, each acquired image contained four channels for the four excitation/emission combinations: Ex405/Em530 and Ex488/Em530 for the GTP sensors, and Ex458/Em630 and Ex594/Em630 for pHRed. One hour before the imaging, cells were rinsed with PBS and replenished with the immunofluorescence-compatible media (IFM) plus drugs or vehicle controls as indicated in figure legends, to equilibrate the cells with the IFM. We captured a minimum of three images per population per treatment and performed ratiometric analysis on 30 cells per population per treatment with ImageJ (NIH) by outlining the individual cells and measuring the mean fluorescence in each channel for each cell. We then calculated the Ex405/Ex488 ratio for the GTP sensors and Ex594/Ex458 ratio for pHRed. We imaged the channels sequentially to minimize the amount of bleed-through. For cells expressing both GTP sensors and pHRed, we corrected images by subtracting 9% of the Ex458 channel values from the Ex405 channel values before analysis; however, corrected and uncorrected data were nearly identical when normalized to controls. To extrapolate the approximate pH from the Ex594/Ex458 ratio we interpolated the underlying data from ref. 17 to create a regression curve where the y -value is the Ex594/Ex458 ratio and the x -value is the pH. The calculated ratios were then used to determine the approximate pH for each cell, an approach that has been proven to be quite reliable¹⁷. For the gradient imaging, we cropped regions containing single cells and calculated ratios between the two channels pixel by pixel with the RatioPlus plugin, with a background subtraction of 10 in the numerator image and a multiplication factor of 2.0. The ratio images were then subjected to a 0.5% contrast enhancement and false-colored with the FIRE_LUT tool. When comparing ratios across the three sensors or over a time course, we blended the images in one stack in ImageJ so that the enhancement manipulation and LUT could be applied uniformly to all images at once. For the short-term treatment with MPA, we pretreated vehicle- and MPA-treated cells overnight with 0.5 mM N-acetyl-cysteine (NAC) to prevent potential short-term induction of ROS by MPA^{31,32}. For the bleaching experiment, the same group of cells was sequentially imaged every 30 s. The Ex405/Ex488 ratio for each time point was calculated and normalized to the ratio at $t = 0$ h. For the continuous time-lapse analysis, the values for GEVAL30 and GEVAL530 were normalized to those for GEVALNull in the same conditions. For HTP analysis, the Z' score was calculated using the formula $Z' = (1 - (3(\sigma_s + \sigma_c)/|\mu_s - \mu_c|))^{33}$. A Z' factor value between 0.5 and 1, between 0 and 0.5, or below 0 indicates an optimal, a marginal or a non-useful assay, respectively.

Statistical analysis. Each experiment was performed at least two independent times (normally between two and four independent

experiments, as specified in each figure legend). Representation of data as dot-plots and bar-and-whisker graphs is described in figure legends. Statistical analysis was performed using two-tailed Student's *t*-test (or, where indicated, two-tailed Mann–Whitney test). A two-tailed *P* value < 0.05 was considered statistically significant for all analyses, and the exact *P* value for each comparison is reported within each figure.

Data availability. The data that support the findings of this study are available from the corresponding authors upon reasonable request. Additional information can be found in the associated **Life Sciences Reporting Summary**.

29. Mannava, S. *et al.* Depletion of deoxyribonucleotide pools is an endogenous source of DNA damage in cells undergoing oncogene-induced senescence. *Am. J. Pathol.* **182**, 142–151 (2013).
30. Bianchi-Smiraglia, A. *et al.* Microphthalmia-associated transcription factor suppresses invasion by reducing intracellular GTP pools. *Oncogene* **36**, 84–96 (2016).
31. Huh, K.H. *et al.* The role of thioredoxin 1 in the mycophenolic acid-induced apoptosis of insulin-producing cells. *Cell Death Dis.* **4**, e721 (2013).
32. Malekinejad, H., Moradi, M. & Fink-Gremmels, J. Cytochrome C and caspase-3/7 are involved in mycophenolic acid-induced apoptosis in genetically engineered PC12 neuronal cells expressing the p53 gene. *Iran. J. Pharm. Res.* **13**, 191–198 (2014).
33. Zhang, J.H., Chung, T.D. & Oldenburg, K.R. A simple statistical parameter for use in evaluation and validation of high throughput screening assays. *J. Biomol. Screen.* **4**, 67–73 (1999).

Life Sciences Reporting Summary

Nature Research wishes to improve the reproducibility of the work that we publish. This form is intended for publication with all accepted life science papers and provides structure for consistency and transparency in reporting. Every life science submission will use this form; some list items might not apply to an individual manuscript, but all fields must be completed for clarity.

For further information on the points included in this form, see [Reporting Life Sciences Research](#). For further information on Nature Research policies, including our [data availability policy](#), see [Authors & Referees](#) and the [Editorial Policy Checklist](#).

Experimental design

1. Sample size

Describe how sample size was determined.

The sample size was determined in consultation with a biostatistician

2. Data exclusions

Describe any data exclusions.

No exclusions

3. Replication

Describe whether the experimental findings were reliably reproduced.

They were reliably reproducible

4. Randomization

Describe how samples/organisms/participants were allocated into experimental groups.

N/A. All work has been done in cultured human melanoma cells.

5. Blinding

Describe whether the investigators were blinded to group allocation during data collection and/or analysis.

N/A.

Note: all studies involving animals and/or human research participants must disclose whether blinding and randomization were used.

6. Statistical parameters

For all figures and tables that use statistical methods, confirm that the following items are present in relevant figure legends (or in the Methods section if additional space is needed).

n/a Confirmed

- The exact sample size (n) for each experimental group/condition, given as a discrete number and unit of measurement (animals, litters, cultures, etc.)
- A description of how samples were collected, noting whether measurements were taken from distinct samples or whether the same sample was measured repeatedly
- A statement indicating how many times each experiment was replicated
- The statistical test(s) used and whether they are one- or two-sided (note: only common tests should be described solely by name; more complex techniques should be described in the Methods section)
- A description of any assumptions or corrections, such as an adjustment for multiple comparisons
- The test results (e.g. P values) given as exact values whenever possible and with confidence intervals noted
- A clear description of statistics including central tendency (e.g. median, mean) and variation (e.g. standard deviation, interquartile range)
- Clearly defined error bars

See the web collection on [statistics for biologists](#) for further resources and guidance.

► Software

Policy information about [availability of computer code](#)

7. Software

Describe the software used to analyze the data in this study.

Image J, Microsoft Excel, GraphPad Prism

For manuscripts utilizing custom algorithms or software that are central to the paper but not yet described in the published literature, software must be made available to editors and reviewers upon request. We strongly encourage code deposition in a community repository (e.g. GitHub). *Nature Methods* [guidance for providing algorithms and software for publication](#) provides further information on this topic.

► Materials and reagents

Policy information about [availability of materials](#)

8. Materials availability

Indicate whether there are restrictions on availability of unique materials or if these materials are only available for distribution by a for-profit company.

No restrictions

9. Antibodies

Describe the antibodies used and how they were validated for use in the system under study (i.e. assay and species).

The following antibodies were used: mouse monoclonal to GAPDH (Cat. # AM4300, Ambion, Austin, TX, USA); rabbit polyclonal to IMPDH2 (Cat # HPA001400, Sigma-Aldrich); and mouse monoclonal to GFP/YFP (Cat # sc-9996, Santa Cruz Biotechnology, Santa Cruz, CA, USA).

10. Eukaryotic cell lines

a. State the source of each eukaryotic cell line used.

SK-Mel-103 human melanoma cell lines were obtained from Sloan Kettering Memorial Cancer Center

b. Describe the method of cell line authentication used.

SK-Mel-103 cells were authenticated at Sloan Kettering Memorial Cancer Center

c. Report whether the cell lines were tested for mycoplasma contamination.

Cells were routinely verified for being mycoplasma-free using MycoAlert mycoplasma detection Kit purchased from Lonza (Allendale, NJ, USA, Cat # LT07-318).

d. If any of the cell lines used are listed in the database of commonly misidentified cell lines maintained by [ICLAC](#), provide a scientific rationale for their use.

N/A

► Animals and human research participants

Policy information about [studies involving animals](#); when reporting animal research, follow the [ARRIVE guidelines](#)

11. Description of research animals

Provide details on animals and/or animal-derived materials used in the study.

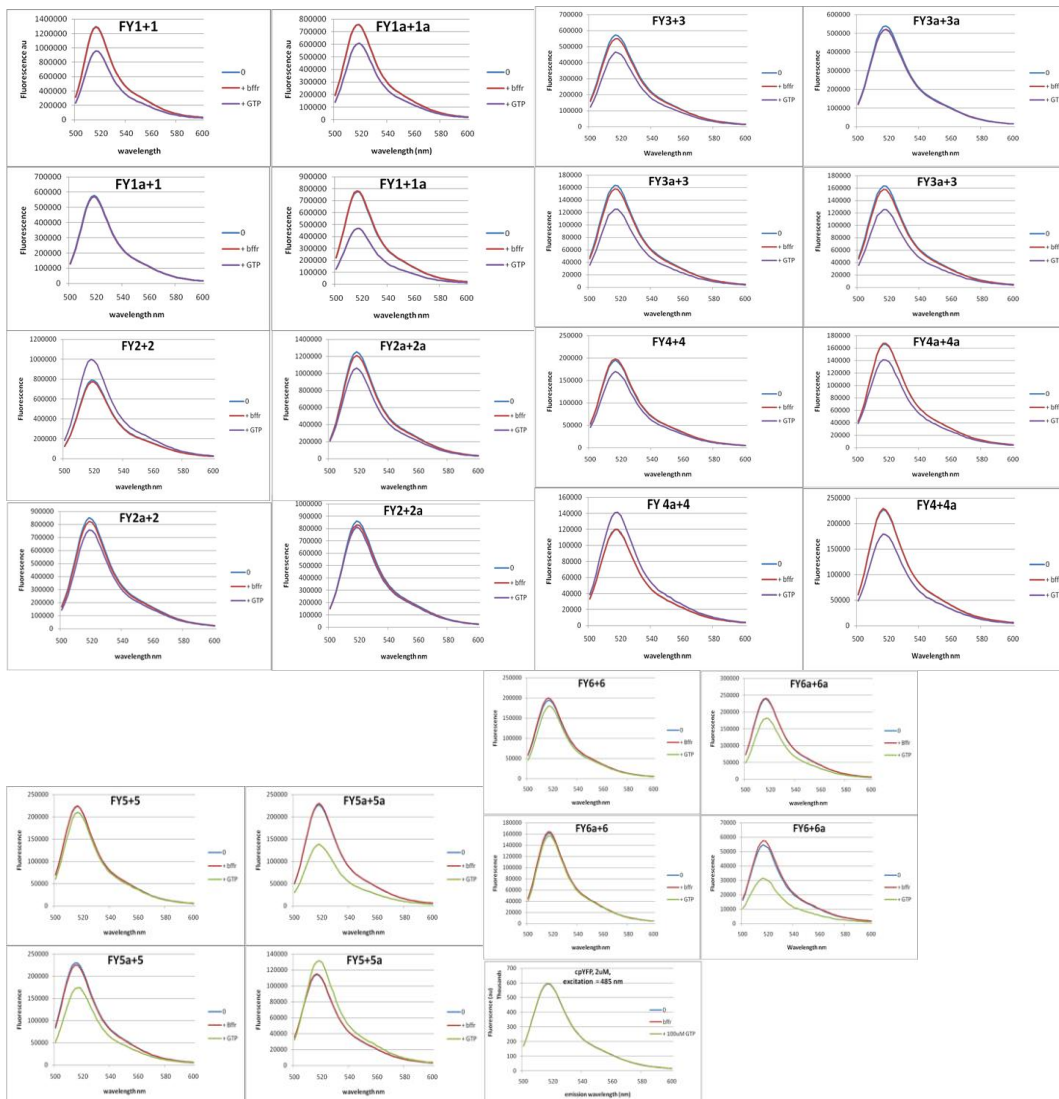
N/A

Policy information about [studies involving human research participants](#)

12. Description of human research participants

Describe the covariate-relevant population characteristics of the human research participants.

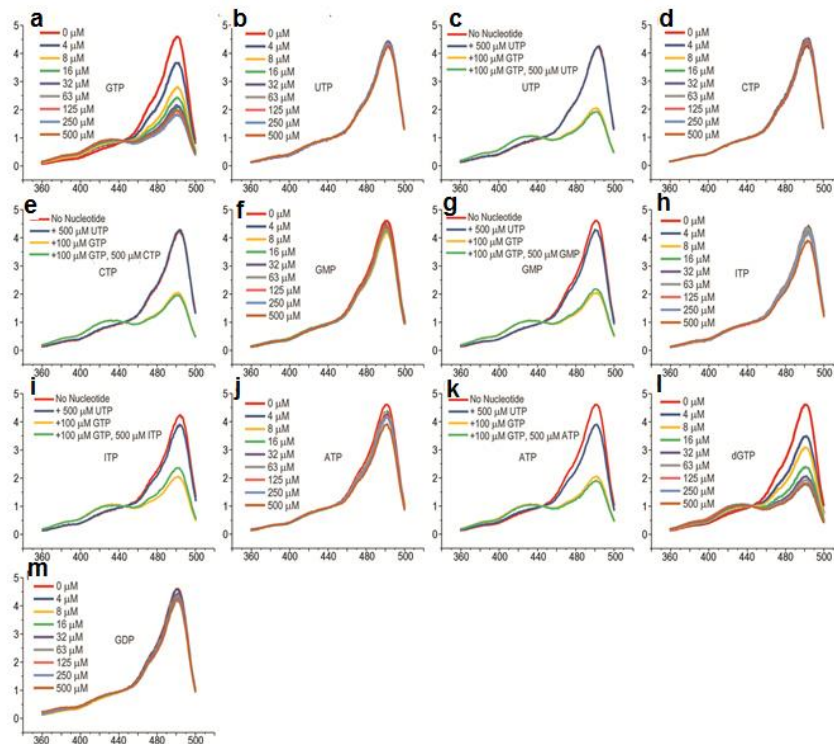
N/A



Supplementary Figure 1

Screening of 24 FeoB–cpYFP fusions for GTP effects on their fluorescence.

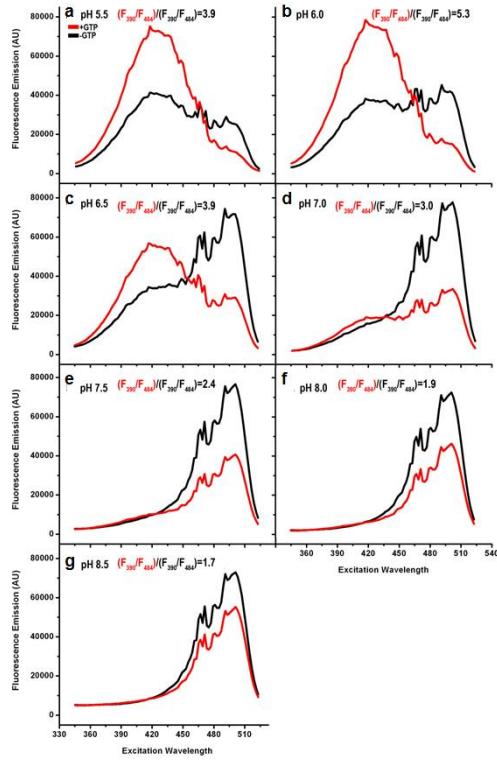
In each panel the emission spectra (500–600 nm) are plotted for the indicated fusions excited at 485 nm and in the absence (blue trace) or presence (red trace) of 100 μM GTP or an equal volume of GTP-free buffer (red trace). Three of the fusions (FY1+1a, FY5a+5a and FY6+6a) show large (>2-fold) reductions in emission upon binding GTP and were selected for further characterization. Fusion nomenclature is as described in main text: the number refers to the position at which the cpYFP was inserted into FeoB, with "1" corresponding to insertion after residue 35 and "6" to insertion after residue 40, and the suffix "a" indicates the addition of an "SAG" or "GT" linker at, respectively, the N- or C-terminus of the cpYFP. The last plot shows the null response of cpYFP alone to GTP.



Supplementary Figure 2

The FY5a+5a fusion is selective for GTP and dGTP.

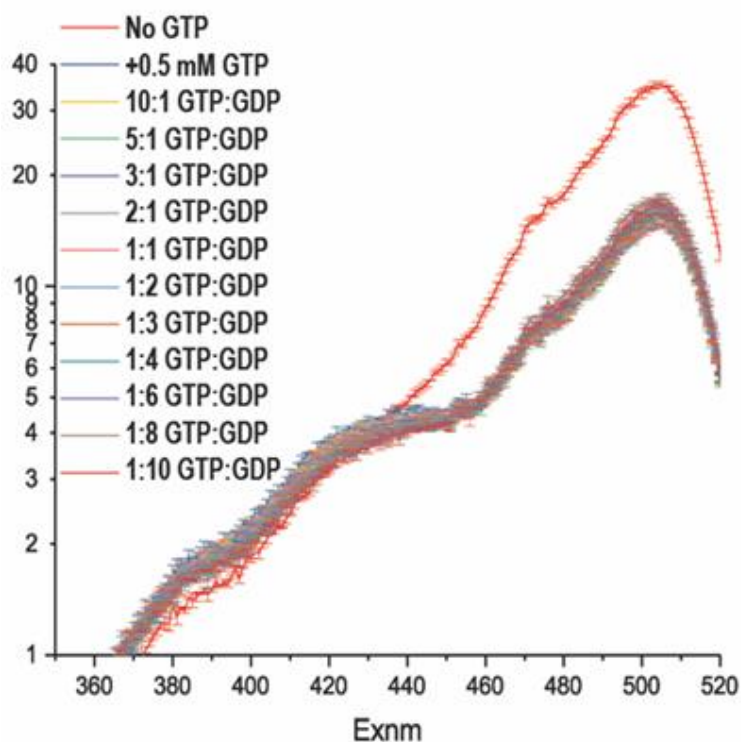
(a) Excitation spectra (360 to 520nm; emission measured at 530nm) of FY5a+5a fusion in the absence (red trace) or presence of 4 (dark blue), 8 (yellow), 16 (green), 31 (purple), 63 (grey), 125 (pink), 250 (light blue) or 500 μ M GTP. (b) As in panel (a), but using UTP rather than GTP. (c) Excitation spectra of FY5a+5a fusion in the absence of nucleotide (red), the presence of 500 μ M UTP (dark blue), 100 μ M GTP (yellow) or 100 μ M GTP and 500 μ M UTP (green) to assess the ability of UTP interfere with the GTP induced spectrum changes. (d) As in (a) but using CTP. (e) As in (c) but with CTP as interfering nucleotide. (f) As in (a) but using GMP. (g) As in (c) but with GMP as the interfering nucleotide. (h) As in (a) but using ITP. (i) As in (c) but with ITP as the interfering nucleotide. (j) As in (a) but using ATP. (k) As in (c) but with ATP as the interfering nucleotide. (l) As in (a) but using dGTP. (m) As in (a) but using GDP.



Supplementary Figure 3

The FY5a+5a fusion exhibits a robust GTP-driven ratiometric change in fluorescence across the physiologically relevant pH range.

(a-g) Plots of the fluorescence emission intensity (at 530 nm) for the FY5a+5a fusion at the indicated pH values vs. excitation wavelength in either the absence (black trace) or presence (red trace) of 1 mM GTP. The ratios of the ratiometric signals ($F_{390\text{ex}}/F_{484\text{ex}}$) +/- GTP vary from 1.7 to 5.3 across the pH 5.5 to 8.5 range.

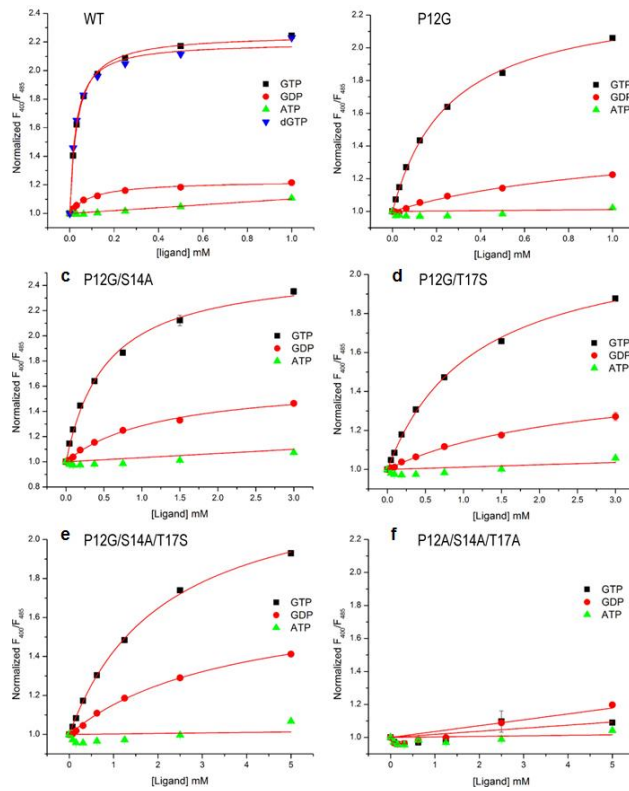


[GTP]:[GDP]	F485/F400
0:0	12 \pm 0.3
0.5mM:0mM	4.3 \pm 0.1
0.5mM:0.05mM (10:1)	4.3 \pm 0.02
0.5mM:0.1mM (5:1)	4.3 \pm 0.1
0.5mM:0.17mM (3:1)	4.4 \pm 0.1
0.5mM:0.25mM (2:1)	4.4 \pm 0.1
0.5mM:0.5mM (1:1)	4.5 \pm 0.2
0.5mM:1mM (1:2)	4.7 \pm 0.1
0.5mM:1.5mM (1:3)	4.9 \pm 0.04
0.5mM:2mM (1:4)	4.9 \pm 0.003
0.5mM:3mM (1:6)	5.4 \pm 0.1
0.5mM:4mM (1:8)	5.6 \pm 0.2
0.5mM:5mM (1:10)	5.4 \pm 0.1

Supplementary Figure 4

Excess GDP does not significantly interfere with GTP sensing.

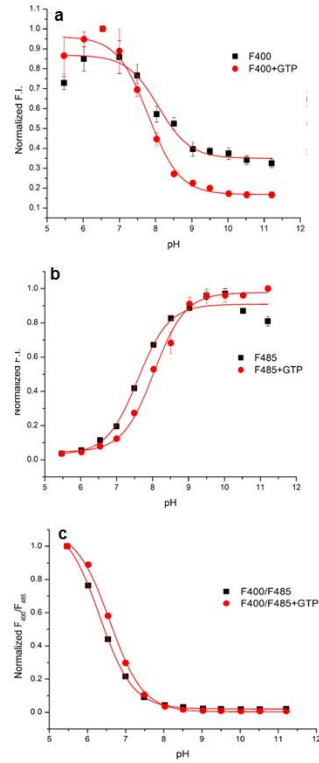
Plots of 530 nm emission intensity (in AU) vs. excitation wavelength for the FY5a+5a fusion in either the absence (red trace) or presence of 0.5 mM GTP and varying concentrations of GDP as indicated (error bars show \pm SEM for n=5 measurements). The 485ex/400ex ratios for the data plotted are given. Addition of 0.5 mM GTP reduces the 485ex/400ex ratio by almost 3-fold while addition of 2mM GDP affects this ratio by less than 10%, and even higher GDP affect this ratio by a maximum of only 25%.



Supplementary Figure 5

Mutations in the FeoB GTP-binding site generate a set of GEVAL sensors that respond to a broad range of GTP concentrations.

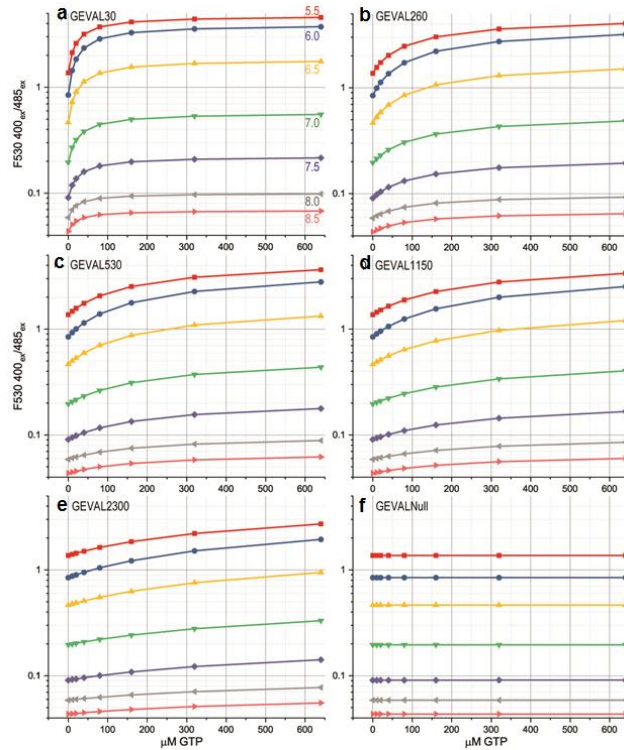
Normalized F_{400ex}/F_{485ex} fluorescence intensity ratios (at 530 nm emission) as a function of variation in the concentration of the indicated ligands are plotted and fit to a Hill equation with offset and cooperativity parameter values of 1.0. Each data point is an average of 3-4 measurements. Error bars are \pm s.e.m. (bars often not visible as spread is smaller than symbol size). (a) GEVAL sensor with WT FeoB component. (b) GEVAL sensor with P12G mutation in FeoB component. (c) GEVAL sensor with P12G/S14A mutation in FeoB component. (d) GEVAL sensor with P12G/T17S mutation in FeoB component. (e) GEVAL sensor with P12G/S14A/T17S mutation in FeoB component. (f) GEVAL sensor with P12A/S14A/T17A mutation in FeoB component.



Supplementary Figure 6

Effect of pH on GEVAL fluorescence.

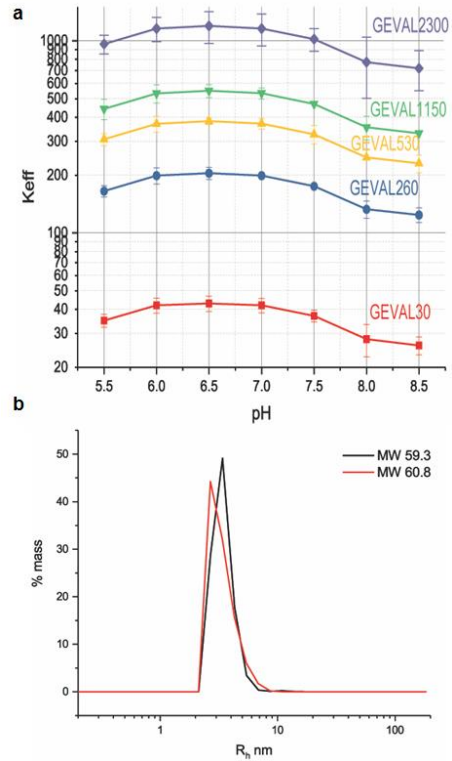
(a) Variation in GEVAL30 530nm fluorescence emission intensity as a function of pH upon excitation at 400nm in either the absence (black trace and square symbols) or presence (red trace and round symbols) of 0.1mM GTP. (b) Variation in GEVAL30 530nm fluorescence emission intensity as a function of pH upon excitation at 485 nm in either the absence (black trace and square symbols) or presence (red trace and round symbols) of 0.1mM GTP. (c) Variation in the ratio of GEVAL30 530nm fluorescence emission intensity as a function of pH when excited at 400 vs. 485 nm in either the absence (black trace and square symbols) or presence (red trace and round symbols) of 0.1mM GTP. In all plots the highest y-value for each data set is normalized to 1.0. Error bars show +/-SEM for n=3.



Supplementary Figure 7

GEVAL sensors exhibit identical responses to pH but varying responses to GTP depending on their GTP affinities.

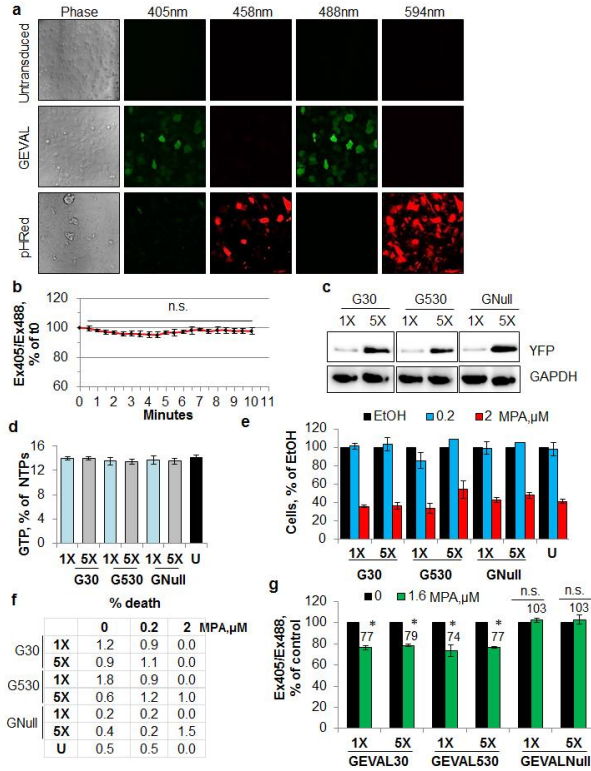
(a) Emission intensity ratios for GEVAL30 at 400nm vs. 485nm excitation plotted against $\mu\text{M GTP}$ at pH 5.5 (red squares), 6.0 (blue circles), 6.5 (yellow upward pointing triangles), 7.0 (green downward pointing triangles), 7.5 (purple diamonds), 8.0 (grey leftward pointing triangles), and 8.5 (pink rightward pointing triangles). (b) As in panel (a) but for GEVAL260. (c) As in (a), but for GEVAL530. (d) As in (a) but for GEVAL1150. (e) As in (a), but for GEVAL2300. (f) As in (a), but for GEVALNull. GEVALNull shows identical pH dependence as other GEVALs but no GTP sensitivity, allowing it to be used as a control to distinguish between fluorescent changes due to GTP vs. pH.



Supplementary Figure 8

Sensor affinities for GTP are relatively constant across physiologically relevant pH ranges.

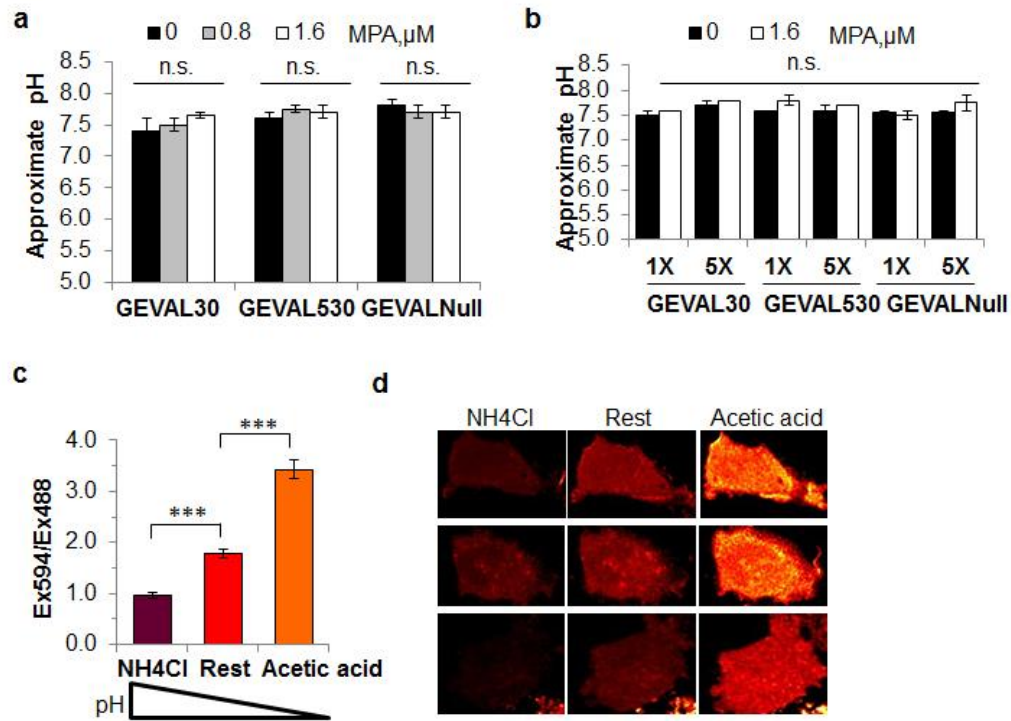
(a) K_{eff} for the GTP induced fluorescence change in GEVAL30 (red trace), GEVAL260 (blue), GEVAL530 (yellow), GEVAL1150 (green) and GEVAL2300 (purple) is plotted as a function of pH (based on data presented in Fig. 3 in main text). The measured K_{eff} values vary by less than $\pm 33\%$ across the specified pH range. Note that these values are based on experiments in which the maximum GTP concentration is $640\mu\text{M}$, which tends to underestimate the K_{eff} for the lower affinity sensors relative to the data (as in Table 1) that includes GTP concentrations that extend well above the sensor K_{eff} . (b) Dynamic light scattering measurements of GEVAL30 in the absence (black trace) or presence (red trace) of 1mM GTP reveal a solution MW and narrow polydispersity profile consistent with a monodisperse monomer under both conditions.



Supplementary Figure 9

Validation of GEVAL sensors in cells.

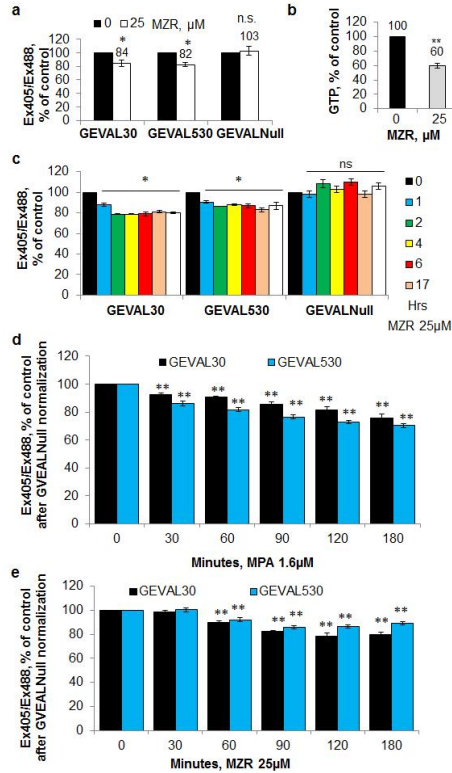
(a) SK-Mel-103 cells were left untransduced or transduced with GEVAL530, or transfected with the pHRed sensor. Cells were imaged with regular light (phase contrast) and excited sequentially at 405nm, 458nm, 488nm, and 594nm (as described in material and methods). (b) GEVAL530-infected cells were monitored for bleaching. The same group of cells was imaged every 30sec for a total of 10 minutes. The Ex405/Ex488 ratio of 10 individual cells was calculated for each time point and the data represents the average \pm standard deviation of these measurements. (c) SK-Mel-103 cells were transduced with two different titers for each GEVAL construct. Increasing amounts of sensors were visualized by immunoblot toward YFP and GAPDH (as a loading control). (d) cells as in (c) were treated for 48hrs with vehicle control or 1.6 μ M MPA. At the end of treatment cell pellets were extracted for nucleotide analysis via HPLC. The data represent the average \pm SEM of two independent experiments. Cells as in (c) were seeded at 200K/well in 6-well plates in duplicates and treated for 48hrs with vehicle control, 0.2 μ M and 2 μ M MPA. At the end of treatment, cells were trypsinized and counted with trypan blue exclusion to determine proliferation (e) and viability (f). The data represent the average \pm SEM of two independent experiments. (g) Cells as in (c) were imaged and the Ex405/Ex488 ratio was calculated for 30cells/population. The data represents the average \pm SEM of 60 cells from two independent experiments. Statistics were performed by two-tailed Student t-Test, * $p < 0.05$; n.s. not significant.



Supplementary Figure 10

Validation of pHRed sensor in cells.

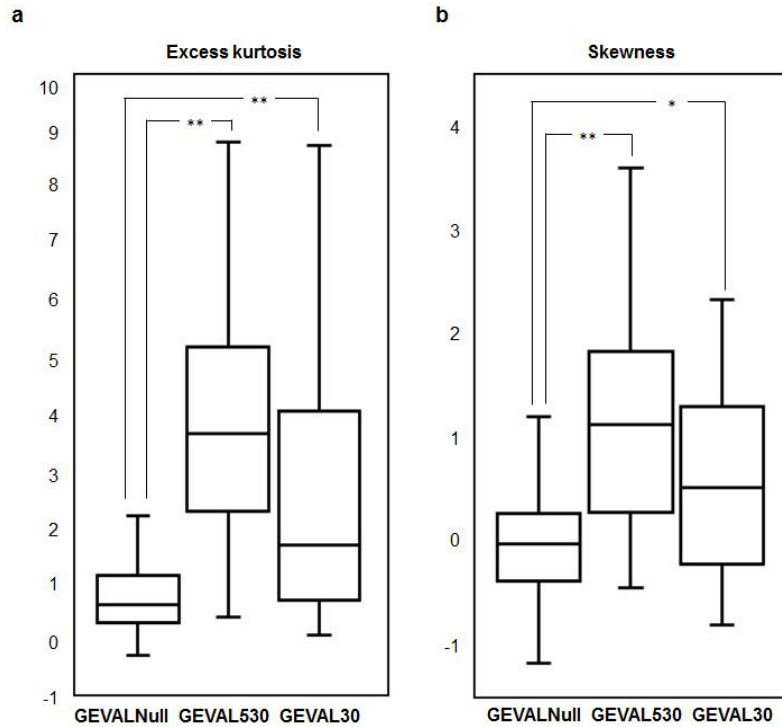
(a) pH analysis by pHRed in SK-Mel-103 cells from Fig 4b,c. The approximate pH for each cell population was calculated using data provided by Dr. Gary Yellen (personal communication). The data represent the average \pm SEM of 60 cells from two independent experiments. (b) pH analysis by pHRed in SK-Mel-103 cells from Supplementary Fig S9g. The data represent the average \pm SEM of 60 cells from two independent experiments. (c) Cells transduced with pHRed vector were imaged sequentially at rest and after treatment with NH₄Cl (20mM final) and acetic acid (10mM final) and the Ex594/Ex488 was calculated. The data represent the average \pm SEM of 25 individual cells from two independent experiments. (d) Representative images from cells as in (c). Statistics were performed by two-tailed Student t-Test, *** $p < 0.0001$; n.s. not significant.



Supplementary Figure 11

Time course of GEVAL sensor activity in response to IMPDH2 pharmacological inhibition by mizoribine.

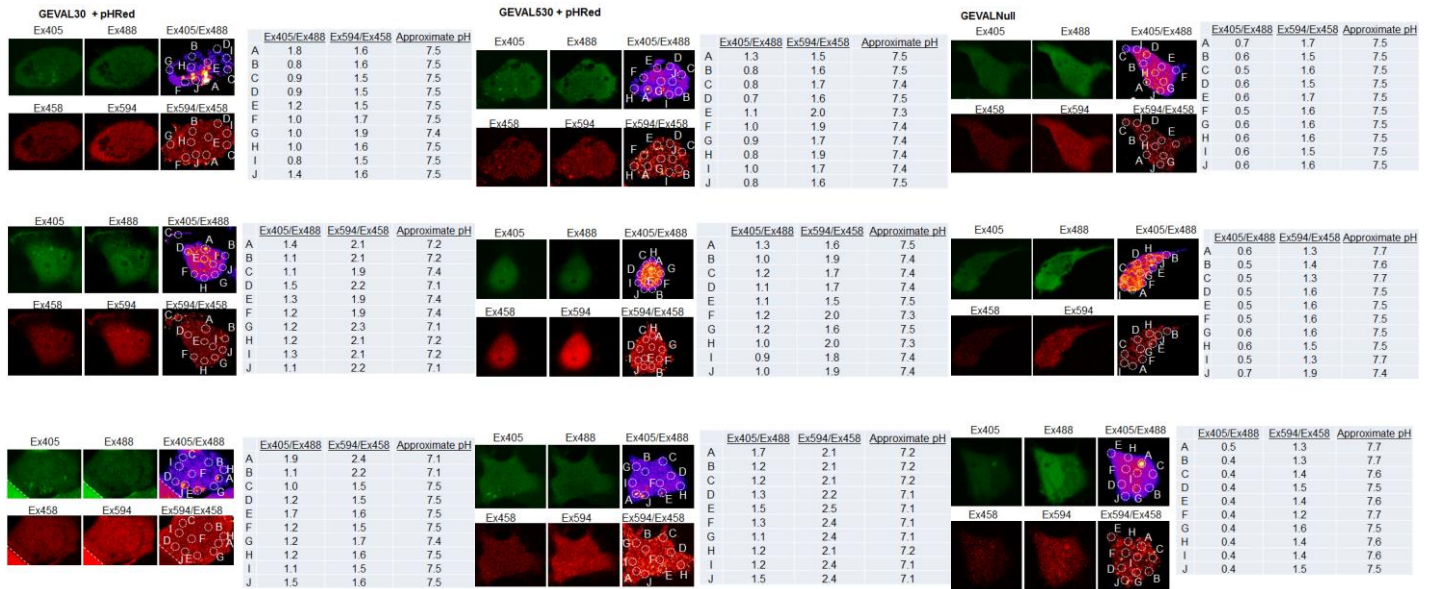
(a) SK-Mel-103 cells transduced with GEVAL30, GEVAL530, or GEVALNull, and treated for 48hrs with 25 μ M MZR. Cells were then imaged and the Ex405/Ex488 ratio was calculated for 30cells/population. The data represent the average \pm SEM of three independent experiments. (b) HPLC analysis of GTP in cells treated as in (a). The data represent the average \pm SEM of 3 independent experiments. (c) SK-Mel-103 cells were transduced with GEVAL30, GEVAL530, or GEVALNull. Cells were plated on coverslip chambers and imaged (0h). Cells were then treated with 25 μ M MZR and cell populations were imaged at the indicated time points to calculate the Ex405/Ex488 ratio in 30 cells/population. The data represent the average \pm SEM of 60 cells from 2 independent experiments. Quantification of Ex405/Ex488 in 10 cells/population over time for cells treated with 1.6 μ M MPA (d) or 25 μ M MZR (e). These measurements are related to the cells shown in Fig. 4. The data represent the average \pm SEM of 20 cells from two independent experiments normalized over the GEVALNull signal and to the untreated control (0h) in each group. Statistics were performed by two-tailed Student t-Test, * $p < 0.05$, ** $p < 0.001$; n.s. not significant.



Supplementary Figure 12

Characteristics of the distribution of signal ratios in cells expressing GEVALs.

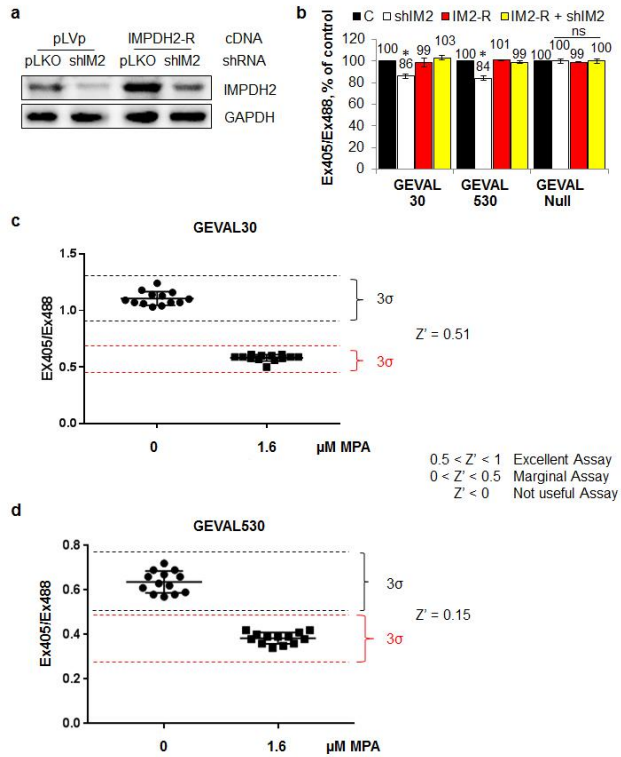
SK-Mel-103 cells transduced with GEVALNull, GEVAL530, or GEVAL30 were imaged and 30 cells were randomly chosen for analysis from each cell population. Pixel-by-pixel ratiometric images were created with ImageJ as described in material and methods and the signal ratio was used to calculate excess kurtosis (a) and skewness (b) for each cells. The bar and whisker plots depict median and quartiles for each parameter. Statistics were performed by two-tailed Mann-Whitney test. * $p < 0.05$, ** $p < 0.001$.



Supplementary Figure 13

Evaluation of GEVALs and pHRed gradients in cells.

SK-Mel-103 cells transduced with GEVALs and pHRed were imaged as described. Pixel-by-pixel ratiometric pictures for the GEVAL wavelengths (Ex450/Ex488) and the pHRed wavelengths (Ex594/Ex458) were generated in ImageJ with the Ratio Plus plug-in. pHRed ratiometric images were false-colored with the RED HOT LUT. Individual wavelengths and their ratio images are presented, along with the ratio values for 10 different areas within each cell and the corresponding approximate pH values.



Supplementary Figure 14

Evaluation of IMPDH2 dependence for shRNA effects and of GEVAL performance for HTP screenings.

(a) SK-Mel-103 cells were transduced with empty vector (pLVp) or an shRNA-resistant IMPDH2 expression vector (IMPDH2-R) and superinfected with an empty vector (pLKO) or shRNA to IMPDH2. The resulting cell populations were then transduced with the three GEVALs. IMPDH2 manipulations were verified by immunoblot and GAPDH was used to verify equal loading (b) cells as in (a) were imaged and quantified. The data represent the average \pm SEM of two independent experiments normalized over the untreated control in each group. SK-Mel-103 cells transduced with GEVAL30 (c) or GEVAL530 (d) were seeded in a glass-bottom 96well plate (3,000cells/well; 26wells/sensor). Half of the wells were treated with vehicle control and half with 1.6 μ M MPA. Wells were imaged at 20X (dry lens) and the Ex405/Ex488 for 10 cells in each well was calculated; the average of the ratio of the 10 cells was used as the mean reading for that well. The Z' factor was calculated using the formula $Z' = (1 - (3 * (\sigma_s + \sigma_c) / |\mu_s - \mu_c|))$, where σ_s and σ_c are the standard deviations of the sample (+MPA) and the control (vehicle), respectively, and μ_s and μ_c are the means of the sample and control, respectively. Statistics were performed by two-tailed Student t-Test, * $p < 0.05$; n.s. not significant.

Supplementary Note 1

To evaluate potential autofluorescence and bleed-through, untransduced cells and cells transduced with only pHRed or one of the GEVAL sensors were imaged using sequential excitation with 405 nm and 488nm for the GEVAL sensors and 458nm and 594nm for the pHRed sensor (see online methods). Untransduced cells were not fluorescent; GEVAL-infected cells gave a robust signal when excited at 405nm and 488nm, and showed a minimal bleedthrough in the 458nm channel of pHRed. Cells transfected with pHRed displayed robust signals at pHRed-specific excitation wavelengths and demonstrated a <9% bleed-through in the 405nm channel for the GEVAL sensors (**Supplementary Fig. S9a**). The GEVAL sensors were also photostable (**Supplementary Fig. S9b**).

Next, cells were transduced with 1X and 5X viral titers for each sensor followed by evaluation of YFP levels by immunoblot (**Supplementary Fig. S9c**). NTP levels were assessed by HPLC and equal amounts of GTP were detected in all cell populations, similarly to untransduced control cells (**Supplementary Fig. S9d**), indicating that GEVAL levels do not affect intracellular GTP pools. Proliferation and viability of 1X and 5X cells were assessed via trypan blue assay 48hrs post-treatment with 0, 0.2 μ M or 2 μ M of mycophenolic acid (MPA), an inhibitor of inosine monophosphate dehydrogenases (IMPDH), that causes depletion of intracellular GTP levels^{18,19}. Uninfected and GEVAL-expressing cells responded similarly to the tested MPA concentrations, (**Supplementary Fig. S9e,f**), indicating that the GEVAL sensors do not affect cells with depleted GTP levels.